

# High- $T_c$ superconductivity through a charge pairing mechanism in a strongly coupled disordered phase.

J.L. Alonso<sup>1</sup>, Ph. Boucaud<sup>2</sup>,  
V. Martín-Mayor<sup>3</sup> and A.J. van der Sijs<sup>4</sup>

April 13, 1998

<sup>1</sup>*Departamento de Física Teórica, Universidad de Zaragoza, 50009 Zaragoza, Spain.*

<sup>2</sup>*LPTHE, Université de Paris XI, 91405 Orsay Cedex, France.*

<sup>3</sup>*Departamento de Física Teórica I, Universidad Complutense de Madrid, 28040 Madrid, Spain.*

<sup>4</sup>*Swiss Center for Scientific Computing, ETH-Zürich, ETH-Zentrum, CH-8092 Zürich, Switzerland.*

**e-mail:** <sup>1</sup>*buj@gteorico.unizar.es*, <sup>2</sup>*phi@qcd.th.u-psud.fr*, <sup>3</sup>*victor@lattice.fis.ucm.es*,

<sup>4</sup>*arjan@scsc.ethz.ch*

## Abstract

We present a lattice field theory of spins coupled to Dirac fermions, as a model for the doped copper oxide compounds. Both the fermionic and spin degrees of freedom are treated dynamically. The influence of the charge carriers on the magnetic ordering follows automatically. The magnetic phase diagram at zero temperature is studied numerically and with Mean-Field methods. The Hybrid Monte Carlo algorithm is adapted to the  $O(3)$  non-linear  $\sigma$  model constraint. The charged excitations in the various phases are studied at the Mean-Field level. Bound states of two charged fermions are found in a strongly coupled *paramagnetic* phase, without requiring a Fermi sea. We acquire a qualitative understanding of high- $T_c$  superconductivity through Bose-Einstein condensation of those dynamically bound pairs. The model also implies insulating behaviour at low doping, and Fermi liquid behaviour at large doping. We predict the possibility of reentrant superconductivity and the absence of superconductivity in spin-1 and spin-3/2 materials.

*Key words:* High temperature superconductors, Strongly correlated fermions, Pairing interactions, Doped oxide compounds

*PACS:* 74.20.-z, 71.27.+a, 74.25.Dw, 75.10.Jm

# 1 Introduction

Since the discovery of the Cu-based high- $T_c$  superconductors [1] there has been a lot of interest in the physics of antiferromagnets doped with holes. The understanding of such a system would allow a unifying picture of the magnetic and superconducting properties of those materials. Some of the properties to be considered are:

1. Superconductivity appears in doped, ceramic materials, like  $\text{La}_2\text{CuO}_4$  doped to  $\text{La}_{2-x}\text{Sr}_x\text{CuO}_4$ , *in a narrow range of doping not too far from the antiferromagnetic insulating state*, at low temperatures.
2. For zero doping fraction,  $x = 0$ , they are insulating antiferromagnets.
3. At large  $x$  they appear to have normal metallic behaviour.
4. They are layered compounds, made up of  $\text{CuO}_2$  planes separated by some “charge reservoir”. The doping suppresses the antiferromagnetic (AFM) correlation between neighboring  $\text{CuO}_2$  planes. However, large ( $\xi \sim 10a$ ) in-plane correlations remain just above  $T_c$ . Also, transport phenomena occur mainly in the  $\text{CuO}_2$  planes, so everything looks like a  $d=2$  problem, *with localized spins on the Cu and mobile holes on the O ions*.
5. As in the conventional superconductors, the superconductivity is charge-2 in nature, suggesting a pairing state.
6. The *normal* (*i.e.* non superconducting) state is anomalous: there is experimental evidence for anomalous behaviour of several response functions (magnetic susceptibility, specific-heat, DC conductivity) in the *normal* phase. This is usually referred to as a *pseudo-gap* phase, for which a picture of a singlet pairing already *above*  $T_c$  is emerging [2]. That is, the pair formation seems to occur *independently* of the quantum liquid condensation (*i.e.* the macroscopic phase coherence), at least for underdoped (*i.e.* superconducting samples less than optimally doped) materials [3].
7. There is a negligibly small isotope effect and there is evidence [4] for a  $d_{x^2-y^2}$  wave pairing state.

The essential questions posed by the phenomenology of the new perovskite superconductors have been phrased as follows in Ref. [5]:

- What is the physical origin of the anomalous *normal* state?
- How can it be characterized?
- What is the mechanism for high- $T_c$  superconductivity?
- What is the pairing state?

We will try to formulate an answer to these questions in the discussion section of this paper.

The behaviour of the undoped compounds (point 2. above) is well understood in terms of the two-dimensional nearest-neighbour quantum antiferromagnetic (AFM) Heisenberg

model. This model can be mapped to the  $O(3)$  non-linear  $\sigma$ -model [6], and the predictions, obtained through renormalization group analysis [7] and chiral perturbation theory [8], agree very well both with experimental [9] data for the cuprates and with numerical [10] data from direct simulation of the AFM Heisenberg model. Therefore, it seems natural to take either the AFM Heisenberg model or the  $O(3)$  sigma model as a starting point to study the doped materials. In contrast with the successful description of the undoped compounds, however, to our knowledge no model has yet been capable of describing the full doping range.

We have recently proposed a simple model [11, 12] which is a natural extension of the  $O(3)$  model to include doped charge carriers. The model is able to explain, at least qualitatively, many of the observed properties of the perovskites from undoped to (highly) overdoped compounds. It is a lattice-regularized, field-theoretical model of interacting spins and Dirac fermions in 2+1 dimensions, with only two free parameters in addition to the temperature: a nearest-neighbour spin coupling and a spin-fermion coupling.

Conceptually, the model has much in common with microscopic spin-fermion Hamiltonians [13], which are somewhat less restrictive than the  $t$ - $J$  model [14]. The formulation of our model as a local lattice field theory has several advantages over those and other models, though. Mean-field (MF) calculations are feasible and, in the absence of a sign problem, numerical Monte Carlo (MC) simulations can be carried out. Our MC results furthermore demonstrate that the MF approximation is quite reliable here.

In the present article we want to present a careful, detailed discussion of the model, its symmetries, and its properties, and give full technical details and results of the MF and MC calculations, some of which were reported in Ref. [11]. In the present paper, our mean-field and numerical studies will be limited to the zero-temperature case, corresponding to infinite Euclidean time direction. However, we will argue on general grounds what happens when the temperature is increased.

The remainder of this paper is laid out as follows. In Section 2 we present our model. In Section 2.1 we discuss the choice of lattice fermions, comment on the symmetries of the model, give its phase diagram and prove the reality of the fermion determinant, even in the presence of a chemical potential. In Section 2.2, we give our interpretation of the model as an effective field theory which tries to embody the essential features of holes strongly coupled to a dynamical AFM spin background, the only fundamental ingredients being symmetries. In Section 3 we examine the phase diagram of the model in the MF approximation. In Section 4 we use MC simulations to complete the study of the phase diagram. For this purpose we have developed a new method that exactly solves the technical problem related to the length-1 constraint on the spin variables [15]. Section 5 is devoted to a study of the relevant excitations in the different phases of the system, at the MF level. A crucial result is the dynamical generation of spin singlet bosonic bound states of charged fermions in the so-called paramagnetic strong (PMS) phase. At the MF level we have not detected any light *fermionic* excitations at *zero* temperature in this PMS phase. Another interesting result is the emergence of fermionic excitations around spatial momenta  $(\pm\pi/2, \pm\pi/2)$  [16, 17], in the low doping AFM phase preceding the superconducting (SC) phase. An important consequence of the paramagnetic nature of our SC phase is that fermionic excitations, if any, *will not center around*  $(\pm\pi/2, \pm\pi/2)$ , while such a behaviour is typical of an AFM phase (see ref. [18] for some recent experimental results). Next, in Section 6.1, we analyze how our model describes the various phenomena in the cuprates at

zero temperature and in Section 6.2 we conjecture the qualitative behaviour of the model at non zero temperature, using arguments based on a few very general thermodynamical properties.

In the Discussion section (Section 7) we will try to answer the essential questions pointed out in Ref. [5] and quoted above. We also reconsider points 1 to 7 as well as the Bose-Einstein (BE) to BCS crossover from the perspective of our model, and we comment on our predictions.

## 2 The model

### 2.1 Motivation, Formulation, Symmetries, Phase Diagram

In order to motivate our model, we start by collecting some of the most compelling pieces of experimental and theoretical evidence and turning them into guidelines for the formulation of the model.

First of all, recall that the undoped parent compounds are described excellently by the 2+1 dimensional O(3) non-linear  $\sigma$ -model [7, 8, 9, 10] (see also Ref. [19]). Therefore, it is very natural to take this as our first guideline:

**A. In the limit of zero doping,  $x = 0$ , our model should reduce to the O(3) non-linear  $\sigma$ -model.**

Another important piece of information comes from point 7 of the list in Section 1. The virtual absence of an isotope effect and the evidence for a  $d_{x^2-y^2}$  wave pairing state favor a mechanism based on spin rather than phonon-mediated pair formation [20, 21]. This leads us to our second guideline:

**B: Our model should be a spin-fermion model** describing fermions of varying mobility interacting with a dynamical background of localized spins.

Next, as emphasized in [22], the general topology of the cuprates phase diagram was in fact first predicted in Ref. [23]. Their point is to assume a strong coupling between the spin of the hole on the oxygen (see point 4) and the spin of the surrounding  $\text{Cu}^{2+}$  ions due to the direct overlap of the wavefunctions. Therefore, from this:

**C: We expect the strong-coupling regime of our spin-fermion model to be the relevant regime** to understand, eventually, the insulating and superconducting phases of cuprates.

Notice that to in order to arrive at **A** and **B** we have essentially used only information from points 2, 4 and 7, while guideline **C** comes from the more general observation that we deal with a strong coupling phenomenon.

Given the above considerations, we have proposed [11] a model defined by the following (2 + 1)-dimensional lattice euclidean (imaginary time) path integral,

$$Z = \int D\phi D\bar{\psi} D\psi \exp(-S) \quad (1)$$

with action,

$$S = - \sum_{x,\mu} k \phi_x \cdot \phi_{x+\hat{\mu}} + \sum_{x,\mu} \frac{\rho}{2} \bar{\psi}_x \gamma^\mu (\psi_{x+\hat{\mu}} - \psi_{x-\hat{\mu}}) + \sum_x \lambda \bar{\psi}_x \phi_x \cdot \tau \psi_x. \quad (2)$$

We use this expression as our starting point, but it should be noted that the model *depends only on the ratio*  $y = \lambda/\rho$ , *through a change in the normalization of the fermion field.* In terms of the effective spin-fermion coupling  $y$ , we get:

$$S = - \sum_{x,\mu} k \phi_x \cdot \phi_{x+\hat{\mu}} + \sum_{x,\mu} \frac{1}{2} \bar{\psi}_x \gamma^\mu (\psi_{x+\hat{\mu}} - \psi_{x-\hat{\mu}}) + \sum_x y \bar{\psi}_x \phi_x \cdot \boldsymbol{\tau} \psi_x. \quad (3)$$

Here  $x$  runs over a  $(2 + 1)$ -dimensional cubic Euclidean space-time lattice. We keep in mind, however, that some coherence perpendicular to the  $\text{CuO}_2$  planes is required to avoid problems with the Hohenberg-Mermin-Wagner theorem at finite temperature, and for a Bose-Einstein condensate to form. Some small supplementary couplings in the orthogonal spatial direction would play this role.

The fields  $\psi$  represent the doped electric charges. Each  $\psi_x$  is a fermionic four-spinor as a shorthand for two flavours of two-component Dirac spinors (we use flavour to mimic the spin, because there is no spin in two spatial dimensions). Each flavour accounts for two components of the four of a  $(3 + 1)$ -dimensional Dirac electron or hole [24]. Both flavours are taken in the same irreducible spinor representation, with  $2 \times 2$  gamma matrices taken as the Pauli matrices  $\sigma^\mu$ . The  $4 \times 4$  matrices  $\gamma^\mu$  in Eq. (3) have the form

$$\gamma^\mu = \begin{pmatrix} \sigma^\mu & 0 \\ 0 & \sigma^\mu \end{pmatrix} \quad \mu = 1, 2, 3. \quad (4)$$

The kinetic term for the fermions is of the nearest-neighbour (hopping) form. Lattice fermions defined in this way undergo species doubling in the perturbative continuum limit [25]. But since all the fermions, the physical one as well as the doublers, decouple in the continuum limit performed in the region of strong spin-fermion coupling [26], the doubling problem is in fact limited to the weakly coupled region. As our only relevant conclusion in this region, the occurrence of Fermi liquid behaviour because of the weak coupling, is not affected by the doublers, we can use these “naive” fermions without any problem. The three-component fields  $\phi$  denote the spins located at the copper ions. They are real scalar bosonic variables, subject to the constraint  $\phi^2 = 1$ , as in the  $\text{O}(3)$  non-linear  $\sigma$ -model. Their kinetic term, a nearest-neighbour hopping interaction, is the field-theoretic equivalent of a Heisenberg superexchange interaction. The last term in Eq. (3) describes the interaction between the spins and the Dirac fermions, which is diagonal in Dirac space. The Pauli matrices  $\tau^a$  act in flavour space.

Let us now consider the symmetries of (3). First of all, we have the usual cubic symmetry, the lattice remnant of  $(2+1)$ -dimensional Euclidean “Lorentz” symmetry. Next there is a discrete parity symmetry, which in  $(2+1)$  dimensions is defined as the reflection of one of the spatial axes, say the  $x$ -axis. Under this parity symmetry, the fermions can be seen to transform as

$$\psi \rightarrow \sigma_1 \psi, \quad \bar{\psi} \rightarrow -\bar{\psi} \sigma_1, \quad (5)$$

so the  $\phi$  field is a pseudoscalar in this sense. In addition, the action (3) is invariant under an  $\text{SU}(2)$  “flavour” symmetry in which  $\psi$  transforms as the fundamental representation and  $\phi$  transforms as the adjoint one. So, our model maintains after doping the well tested symmetry of the  $\text{O}(3)$  non-linear  $\sigma$ -model describing the undoped material [9]. Note that by requiring the two fermion flavours to have the same Lorentz structure (that is, by

choosing the  $\gamma$ 's as in (4)) no fermion mass term is allowed which preserves the above symmetries [27].

There are two more discrete symmetries of our model (3), which will be useful in the MF calculation of the phase-diagram. The first one is

$$Z(k, y) = Z(k, -y), \quad (6)$$

which becomes clear if we make the change of variables

$$\psi_x \rightarrow \exp\left(i\frac{\pi}{2}\epsilon_x\right) \psi_x, \quad \bar{\psi}_x \rightarrow \exp\left(i\frac{\pi}{2}\epsilon_x\right) \bar{\psi}_x, \quad (7)$$

where

$$\epsilon_n = (-1)^{\sum_{\mu} x_{\mu}}. \quad (8)$$

This implies that  $Z(k, y)$  is a function of  $y^2$  only and we can restrict ourselves to  $y > 0$ .

In addition, there is a symmetry

$$Z(k, y) = Z(-k, -iy), \quad (9)$$

as can be seen by making the substitutions

$$\psi_x \rightarrow \exp\left(i\frac{\pi}{4}\epsilon_x\right) \psi_x, \quad \bar{\psi}_x \rightarrow \exp\left(i\frac{\pi}{4}\epsilon_x\right) \bar{\psi}_x, \quad \phi_x \rightarrow \epsilon_x \phi_x. \quad (10)$$

The latter symmetry implies that the lattice regularization of the non-linear  $\sigma$ -model,  $y=0$  (or  $y=\infty$ , see Sections 3, 4), is equally valid in a ferromagnetic or an antiferromagnetic phase. This will be of fundamental importance in section 2.2.

In order to perform computations in field theoretical models of this type, one has to integrate out the fermion fields; the reason being that they are anticommuting Grassmann fields, while both in MF and in MC one needs to be able to work with a c-number ordering. This integration leads to a  $\phi$ -dependent determinant which is called the fermion determinant. It is important to know whether this determinant is a real number. To study this, let us write down the original fermion matrix (Latin letters  $x, y, \dots$  will refer to lattice points,  $i, j, \dots$ , will represent flavour indices, while Greek letters  $\alpha, \beta, \dots$  are used for Dirac indices):

$$\hat{M}_{x\alpha i; y\beta j} = K_{x\alpha i; y\beta j} + Y_{x\alpha i; y\beta j}, \quad (11)$$

$$K_{x\alpha i; y\beta j} = \frac{1}{2} \sum_{\mu} (\delta_{x+\mu, y} - \delta_{x-\mu, y}) \sigma_{\alpha\beta}^{\mu} \delta_{ij}, \quad (12)$$

$$Y_{x\alpha i; y\beta j} = y \delta_{xy} (\boldsymbol{\phi} \cdot \boldsymbol{\tau})_{ij} \delta_{\alpha\beta}. \quad (13)$$

Keeping in mind that for Pauli matrices  $\sigma_2 \sigma_i \sigma_2 = -\sigma_i^*$ , where \* means complex conjugation, and that  $[\boldsymbol{\gamma}, \boldsymbol{\tau}] = 0$ , one easily proves that, for real  $y$ ,

$$\sigma_2 \tau_2 (K + Y) \sigma_2 \tau_2 = -(K^* + Y^*). \quad (14)$$

Therefore,

$$\det(K + Y) = \det(-K^* - Y^*) = [\det(K + Y)]^*, \quad (15)$$

*i.e.* the determinant is real. Thus, by doubling the number of fermion families, we obtain a positive determinant. Had we introduced a chemical potential,  $\mu$ , the only change would be the introduction of  $e^{\pm\mu}$  on the temporal links of the kinetic matrix [28]. The essential requirement for Eq. (14) to hold (that the only non-real numbers are in  $\gamma, \tau$ ) is thus not endangered by the chemical potential and the determinant is still real.

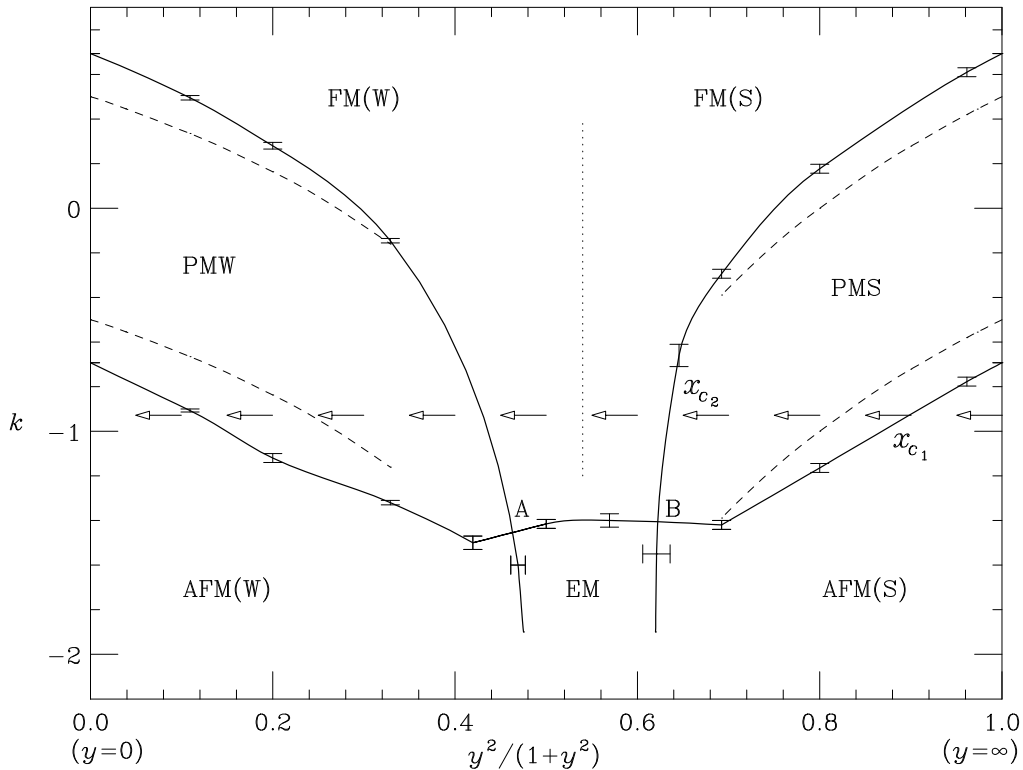


Figure 1: Phase diagram of the action (3), for two fermion families. Dashed lines are from the MF calculation, solid lines from a MC calculation on an  $8^3$  lattice. The arrows indicate the doping-“trajectory”.

The phase diagram of the model at zero temperature is shown in fig. 1. Notice that it is very similar to the phase diagram of (chiral) Yukawa models for the electroweak sector of the Standard Model of elementary particle interactions [29]. At  $y = \infty$  and at  $y = 0$  we recover the non-linear  $\sigma$ -model (see sections 3,4) with its well known paramagnetic (PM), ferromagnetic (FM) and antiferromagnetic (AFM) phases. At finite  $y$ , we expect these phases to extend into the  $(k,y)$  plane. One of its most important features is that there are two mutually disconnected paramagnetic phases, one at weak coupling (called PMW) and one at strong coupling (PMS). One sees that the PMW-FM and the PMW-AFM transition lines meet in a point **A**, where this disordered phase ends. In the strong coupling sector of the phase diagram, a similar behaviour is found, with the two transition lines meeting at point **B**. This observation means that one may expect totally different behaviour in each of the two paramagnetic phases. This is indeed the case, as we shall see later.

As there is no evidence for a phase transition between the strong- and weak-coupling regions of the FM and AFM phases, we name them FM(W) and FM(S), AFM(W) and AFM(S) (note the parentheses). There may be crossovers between these regions, though.

Between the points **A** and **B**, we find a phase where both the magnetization and the staggered magnetization are different from zero. We name this phase *exotic magnetic* (EM). An appealing possibility is that it corresponds to a helicoidal phase. This would merit a more detailed study (see section 6.1 for some comments on this point). We expect the EM phase to disappear for large enough  $-k$ , but we have not explored this numerically.

## 2.2 Phenomenological use of the model

Before embarking on a detailed study of the model, let us briefly discuss its relation with the phenomenology of the cuprates. In particular, it is important to explain how the doping fraction  $x$  is accounted for by the model.

By increasing the doping fraction, one increases the overall mobility of the charge carriers. In our model, this mobility is embodied in the fermionic hopping parameter  $\rho$  in (2). The exact mapping between  $x$  and  $\rho$  is not important for the qualitative description, but it is important that in the limit  $x, \rho \rightarrow 0$  one recovers the O(3) model of the undoped compounds (cf. guideline A. in Section 2.1). Thus, the undoped compound will be described by  $y = \lambda/\rho = \infty$ , and the large- $y$  regime corresponds to the strongly-correlated small- $x$  region, with immobile, localized carriers [30].

Within the lattice O(3) model, we still have two possible points to describe the undoped materials (see fig. 1). One in the FM phase and one in the AFM phase, related by symmetry (9). Although one usually considers the FM phase, especially in continuum descriptions, it is perfectly legitimate (see Eqs. (9,10) and comments below it) to consider the AFM phase. In fact, as the doping is experimentally known to destroy the antiferromagnetism, this turns out to be the most natural option (see fig. 1). (Let us remark though, that the reader can start in the ferromagnetic phase if he/she so wishes, by taking an imaginary coupling constant, as in Eq. (9)).

The most important effect of changing the doping fraction,  $x$ , will be a change in the effective spin-fermion coupling,  $y$  (indicated by the arrow-line in figure 1), and therefore a change of the system ground state and excitations (fermionic and bosonic). Strictly speaking however, there will be a relation between  $x$  and a chemical potential,  $\mu$ , which in fact could be introduced in our formulation (recall that the fermion determinant would remain real). This relation would be in addition to the (phenomenological) relation between  $x$  and  $(y, k)$ . We will now argue, though, that for the physics considered in this paper we can ignore the chemical potential. In other words, a possible chemical potential would not change the excitations of the ground state in any essential way.

Let us start with a general point, that our model captures the insertion of charge carriers in an effective way, by increasing the overall mobility. One could object to this that a vanishing chemical potential entails the absence of a Fermi surface. In the strong-coupling region, however, there are two possible responses to this objection. First of all, for small to intermediate  $x$ , (*i.e.* before and just after superconductivity appears) the very concept of a Fermi surface is very problematic from the experimental point of view [18]. Second, it will turn out that the Fermi surface plays no role in our mechanism to form bound charge pairs. Therefore, ignoring a possible chemical potential in the small- $x$  region,

whose main role would have been to fix the Fermi surface, is perfectly consistent, both with the experimental situation and within the context of the dynamical pair formation in our model.

The overdoped, large- $x$  region, on the other hand, is characterized by Fermi liquid behaviour, so the presence of a chemical potential in the small- $y$  region of our model will be essential to determine the thermodynamics of the system. Since the only statement we want to make concerning this large- $x$  region is the actual emergence of this Fermi liquid behaviour, we can forget about the chemical potential also in the large- $x$  region, for our present purposes.

In the superconducting regime, finally, a chemical potential would change to some extent the ground state and the excitations of the system. However, one expects that in a region of heavy fermions, a quenched region, this change will be small. So we can drop the chemical potential here too.

After having discussed the phenomenological use and interpretation of the model defined by (2), we shall proceed to solve it.

### 3 Mean Field Calculations of the Phase Diagram

Our aim in this section is to determine the zero-temperature phase diagram of the model in the  $y$ - $k$  plane (cf. Fig. 1), using Mean Field techniques. These calculations already provide a lot of insight, especially for the strong coupling region. They will be contrasted with numerical simulations for the phase diagram in Sect. 4, and they will be extended to a study of the relevant charged (quasi-particle) excitations in Sect. 5.

Our Mean Field calculations are based on small- and large- $y$  expansions combined with the saddle point methods described in Ref. [31]. This approach guarantees a systematic expansion in  $1/d$ , which is particularly important for operators which are zero to lowest-order. Our particular method furthermore allows us to handle (products of) fermionic variables occurring in the expansion of the fermion determinant in a well-defined way. These techniques have been developed and applied in the context of similar lattice models [32, 33] of the Electroweak sector of the Standard Model of elementary particle interactions.

We shall first concentrate on the small- $y$  region, and incorporate the fermion determinant up to  $\mathcal{O}(y^2)$ .

In order to apply the saddle-point method, the integration over the fields must be unrestricted. We therefore need to replace the integration over the spin vectors  $\phi$ , constrained by the condition  $|\phi| = 1$ , with an integration over unconstrained variables  $\xi$ . This is done by multiplying the functional integrand in Eq. (1) by

$$\begin{aligned} 1 &= \int D\xi \delta(\phi - \xi) \equiv \prod_n \prod_{a=1}^3 \int_{-\infty}^{\infty} d\xi_x^a \delta(\phi_x^a - \xi_x^a) \\ &= \prod_x \prod_{a=1}^3 \int_{-\infty}^{\infty} d\xi_x^a \int_{-\infty}^{\infty} \frac{dA_x^a}{2\pi} \exp[iA_x^a(\phi_x^a - \xi_x^a)] , \end{aligned}$$

and replacing a conveniently chosen subset of the  $\phi$  variables in the action  $S$  with  $\xi$  fields.

We obtain

$$\begin{aligned}
Z &= \int \frac{D\xi DA}{(2\pi)^3} \exp \left[ k \sum_{x,\mu} \xi_x \cdot \xi_{x+\mu} - i \sum_x \mathbf{A}_x \cdot \xi_x \right] \\
&\times \int D\bar{\psi} D\psi \exp \left[ - \sum_{x,\mu} \frac{1}{2} \bar{\psi}_x \gamma^\mu (\psi_{x+\hat{\mu}} - \psi_{x-\hat{\mu}}) \right] \\
&\times \prod_x \left\{ \int \frac{d\phi_x}{4\pi} \exp [i\mathbf{A}_x \cdot \phi_x - y \bar{\psi}_x \phi_x \cdot \vec{\tau} \psi_x] \right\}.
\end{aligned} \tag{16}$$

Note that both the  $\xi$  fields and the auxiliary fields  $\mathbf{A}$  are unconstrained.

Now we have to integrate out the constrained variables  $\phi_n^a$  (as well as the fermions), before the mean fields can be introduced. Let us concentrate on a single  $\phi_n$  integration in Eq. (16), dropping the subscripts  $n$  for simplicity. First, we perform an expansion in powers of  $y$ . We can write

$$\begin{aligned}
&\int \frac{d\phi}{4\pi} \exp [i\mathbf{A} \cdot \phi - y \bar{\psi} \phi \cdot \vec{\tau} \psi] \\
&= \exp [u(i\mathbf{A})] \exp \left[ -y Q^a \cdot \langle \phi^a \rangle_{i\mathbf{A}} + \frac{1}{2} y^2 Q^a Q^b T^{ab} + \mathcal{O}(y^3) \right],
\end{aligned} \tag{17}$$

where we have defined

$$Q^a = \bar{\psi} \tau^a \psi, \quad u(i\mathbf{A}) = \ln \int \frac{d\phi}{4\pi} \exp [i\mathbf{A} \cdot \phi], \quad T^{ab} = \langle \phi^a \phi^b \rangle_{i\mathbf{A}} - \langle \phi^a \rangle_{i\mathbf{A}} \langle \phi^b \rangle_{i\mathbf{A}},$$

and we have introduced the notation

$$\langle O \rangle_{i\mathbf{A}} = \int \frac{d\phi}{4\pi} O \exp [i\mathbf{A} \cdot \phi] / \int \frac{d\phi}{4\pi} \exp [i\mathbf{A} \cdot \phi].$$

In addition, we introduce a Hubbard-Stratonovich vector parameter  $\lambda$  to deal with the quartic fermion term in Eq. (17),

$$\begin{aligned}
\exp \left[ \frac{1}{2} y^2 \sum_{a,b} Q^a Q^b T^{ab} \right] &= \int \frac{d\lambda}{(2\pi)^{3/2}} \exp \left[ -\frac{1}{2} \sum_a \lambda^a \lambda^a \right] \\
&\times \exp \left[ y \sum_{ab} (\sqrt{T})^{ab} Q^a \lambda^b \right].
\end{aligned} \tag{18}$$

(Note that the matrix  $T$  is self adjoint, and positive definite if  $\mathbf{A}$  is imaginary, so the square root is well defined). Thus, up to this order in  $y^2$ , the action is bilinear in the fermion fields.

Carrying out the fermion integration in Eq. (16) now gives  $\det M$ , where

$$M_{x,\alpha,i;y,\beta,j} = K_{x,\alpha,i;y,\beta,j} + y \delta_{xy} \delta_{\alpha\beta} \sum_a (\langle \phi_x^a \rangle_{iA_x} - \sum_b (\sqrt{T_x})^{ab} \lambda^b) \tau_{ij}^a. \tag{19}$$

The matrix  $K$  has been defined in Eq. (12).

The mean fields are the field values at the saddle point of the free energy

$$-F = \sum_x u(i\mathbf{A}_x) + k \sum_{x,\mu} \boldsymbol{\xi}_x \cdot \boldsymbol{\xi}_{x+\mu} - i \sum_x \mathbf{A}_x \cdot \boldsymbol{\xi}_x - \frac{1}{2} \sum_x \boldsymbol{\lambda}_x^2 + \text{Tr} \log M. \quad (20)$$

A choice of the mean fields should be done at this point, as we cannot calculate  $\log M$  for general  $\{\mathbf{A}_x, \boldsymbol{\lambda}_x\}$ . An appropriate choice for the study of a PM-FM phase transition is

$$\begin{aligned} \mathbf{A}_x &= (0, 0, -i\alpha), \\ \boldsymbol{\xi}_x &= (0, 0, v), \\ \boldsymbol{\lambda}_x &= (0, 0, \lambda), \end{aligned} \quad (21)$$

in terms of which ( $N$  is the lattice volume)

$$F/N = -u(\alpha) - kdv^2 + \alpha v + \frac{1}{2}\lambda^2 - \frac{1}{N} \text{Tr} \log M, \quad (22)$$

with  $\alpha$ ,  $v$  and  $\lambda$  satisfying the saddle point equations

$$\nabla F|_{(\alpha,v,\lambda)} = 0. \quad (23)$$

The fermion matrix,  $M(\alpha, v, \lambda)$ , can be calculated in momentum space, where it is diagonal in its momentum indices. One easily finds

$$\det M = \exp \left[ 2 \sum_p \log \frac{\sum_{\mu=1}^3 \sin^2 p_\mu + y^2 \left( u'(\alpha) - \lambda \sqrt{u''(\alpha)} \right)^2}{\sum_{\mu=1}^3 \sin^2 p_\mu} \right], \quad (24)$$

where we have divided out the determinant for free fermions. We need only the leading  $\mathcal{O}(y^2)$  contribution to the exponent, hence the mean field free energy becomes, in the infinite volume limit:

$$F/N = -u(\alpha) - kdv^2 + \alpha v + \frac{1}{2}\lambda^2 - 2y^2 \left( u'(\alpha) - \lambda \sqrt{u''(\alpha)} \right)^2 C_0, \quad (25)$$

where

$$C_0 = \int_{-\pi}^{\pi} \frac{d^3 p}{(2\pi)^3} \frac{1}{\sum_{\mu=1}^3 \sin^2 p_\mu} = 1.0109240. \quad (26)$$

Next, we shall discuss the actual solutions to Eqs. (23). From  $u(\alpha) = \ln(\sinh \alpha/\alpha)$ , one easily finds that  $\alpha = v = \lambda = 0$  always fulfill them. For small  $k$ ,  $y$ , it is a true minimum of the free energy. This characterizes a paramagnetic (PM) phase, since none of the fields develops an expectation value.

For larger values of  $k$  and  $y$ , there is another, non-trivial solution, corresponding to a ferromagnetic (FM) phase. It emerges when a negative mode in  $F/N$  starts to develop, as a function of the mean fields, and the transition between the two regions is given by the condition ( $F''$  is the Hessian matrix)

$$\det F''|_{(\alpha=0,v=0,\lambda=0)} = 0. \quad (27)$$

This condition is satisfied for  $F/N$  of Eq. (25) if

$$k = \frac{3}{2d} - \frac{2C_0}{d}y^2. \quad (28)$$

This curve defines the phase transition line between the PM and FM phases in the small- $y$  region. Using the symmetry (9), we deduce that there is a similar transition separating the PM and AM phases,

$$k = -\frac{3}{2d} - \frac{2C_0}{d}y^2. \quad (29)$$

Let us finally remark that in the presence of  $N_f$  such fermion fields we would have  $N_f$  factors of  $\det M$ , leading to a multiplication of  $C_0$  by  $N_f$  in Eqs. (28) and (29).

The large- $y$  region is easier to deal with. Here it is convenient to integrate out the fermions directly in Eq. (16), leading to (summation over repeated index is carried)

$$\det M_{x,\alpha,i;y,\beta,j} = \det \left( K_{x,\alpha,i;y,\beta,j} + y\delta_{\alpha\beta}\delta_{xy} \sum_a \phi_x^a \tau_{ij}^a \right) \quad (30)$$

$$= \det \left( y\delta_{\alpha\gamma}\delta_{xz} \sum_a \phi_x^a \tau_{ik}^a \right) \\ \times \det \left( \delta_{zy}\delta_{\gamma\beta}\delta_{kj} + \frac{1}{y} \sum_b \phi_x^b \tau_{kl}^b K_{z,\gamma,l;y,\beta,j} \right). \quad (31)$$

Here we have used that  $(\sum_a \phi^a \tau^a)^2 = \mathbf{1}$  (recall the  $\phi$ 's are unit vectors). Now we can expand  $\log(\det M)$  in powers of  $1/y$ . The  $\mathcal{O}(1/y)$  term vanishes by virtue of  $K_{xx} = 0$ . To second order one obtains

$$\log \det M = \log y^{4N} + \text{Tr} \left( -\frac{1}{2y^2} \sum_a \phi_x^a \tau_{ki}^a K_{x\alpha i;t\gamma l} \sum_b \phi_t^b \tau_{lj}^b K_{t\gamma j;y\beta p} \right) \quad (32)$$

$$= \log y^{4N} + \frac{1}{y^2} \sum_{x,\mu} \phi_x \cdot \phi_{x+\hat{\mu}}. \quad (33)$$

Here,  $\log y^{4N}$  is an irrelevant constant that can be dropped. Notice also that this expression will acquire a prefactor  $N_f$  if there are  $N_f$  identical fermion flavours. One sees that, up to  $\mathcal{O}(1/y^2)$ , the only effect of the fermion determinant is a renormalization of the scalar hopping parameter of the O(3) model,

$$k \rightarrow k + N_f \frac{1}{y^2}. \quad (34)$$

Note that we did not introduce any mean fields to derive this result. The usual MF treatment of the O(3) model with this renormalized coupling now immediately gives us the required phase transition lines in the large- $y$  region of our model:

$$k = \pm \frac{3}{2d} - N_f \frac{1}{y^2}. \quad (35)$$

It is interesting to compare the small- and large- $y$  results, to leading order in  $1/d$ . As is well known, the first order in this expansion is equivalent to any MF approximation, up to higher-order terms. For this purpose, we need the  $1/d$  expansion of the constant  $C_0$  in Eq. (26), which can be calculated as follows:

$$C_0(d) = \int_{-\pi}^{\pi} \frac{d^d p}{(2\pi)^d} \frac{1}{\sum_{\mu=1}^d \sin^2 p_{\mu}} = 2 \int_0^{\infty} ds (e^{-s} I_0(s))^d \quad (36)$$

$$= \frac{2}{d} \left( 1 + \frac{1}{2d} + \mathcal{O}\left(\frac{1}{d^2}\right) \right), \quad (37)$$

where  $I_0(s) = \int_{-\pi}^{\pi} (d\theta/2\pi) \exp(s \cos \theta)$  is the modified Bessel function. In fact, the second equality in Eq. (36) was used to obtain the numerical result (26) for  $C_0$ .

Keeping only the leading-order term  $2/d$  for  $C_0$  we find that the phase transition lines would meet at  $y^2 = 2/d$ .

Now we are ready to map out the phase diagram of the model, as predicted by the MF method for the weak and strong coupling regions. This is done in Fig. 1. The vertical axes at  $y = 0$  and  $y = \infty$  correspond to the O(3) model, with its disordered (PM) and ordered (FM and AFM) phases. These phases extend into the  $y$ -direction, both for  $y > 0$  and  $y < \infty$ . Note that all the phase transition lines bend downward. This can be understood intuitively by assuming a MF value for the fermion condensate, which would act as an external field tending to align the spins  $\phi$  in parallel.

## 4 Monte Carlo: Method and Results

A well established method for dynamical fermion simulations is Hybrid Monte Carlo (HMC) [34]. However, the implementation of this algorithm in a model with constrained variables is not straightforward. This has been satisfactorily achieved for models with variables belonging to a Lie group [35], like  $SU(N)$  gauge theories or like some spin-models, such as the  $O(N = 2, 4)$  non-linear  $\sigma$ -models. However, for other spin variables (not in a Lie group), as in the O(3) non-linear  $\sigma$ -model, this had not been satisfactorily solved yet, although the problem arose already in the first simulations using the Langevin algorithm [15]. Our solution is a generalization of the strategy in [35].

We shall first discuss our solution in the quenched approximation, where comparison with other algorithms is possible (Section 4.1), and then deal with the full theory in Section 4.2. Finally our Monte Carlo results for the phase diagram of the full theory will be presented in Section 4.3.

### 4.1 The HMC method for the quenched approximation

For the purpose of discussion it will prove convenient to briefly describe the HMC method for unconstrained bosonic variables  $\phi(x)$  with action  $S_B(\phi)$  (see ref. [36] for a pedagogical presentation):

1. Introduce uncorrelated gaussian variables  $\pi(x)$  of unit variance (the *conjugate momenta* for the fields  $\phi$ ) and define a Hamiltonian

$$H = \sum_x \frac{1}{2} \pi^2(x) + S_B(\phi). \quad (38)$$

One can then use the hamiltonian equations of motion

$$\begin{aligned} \dot{\phi}(x, \tau) &= \pi(x, \tau), \\ \dot{\pi}(x, \tau) &= -\frac{\delta S_B}{\delta \phi(x, \tau)}, \end{aligned} \quad (39)$$

to perform a microcanonical Molecular Dynamics evolution in “Monte Carlo time”,  $\tau$ . After a certain period of MC time (called “trajectory”), new random momenta  $\pi(x)$  are chosen (“refreshing” the momenta). The crucial properties of Eqs. (40) are their time reversibility, and the invariance of the Liouville measure,  $D\phi D\pi$ , under time evolution.

2. In practice, the molecular dynamics equations of motion for a trajectory are discretized into  $N$  steps  $\Delta\tau$ . This is done using a leap-frog algorithm which is *exactly* time reversible, but does introduce a systematic error which shows up as a non-zero  $\Delta H = \mathcal{O}(\Delta\tau^2)$ . The *detailed-balance* is not endangered by this error, because a Metropolis acceptance step is performed. For fixed trajectory length,  $N$  can then be tuned to optimize the overall efficiency.

To generalize the method to constrained variables, one needs to appropriately define the conjugate momenta and the equations of motion in order to preserve the constraint and, most importantly, not to spoil the time reversibility. Each spin variable,  $\phi$ , lives on the surface of a two-sphere, and correspondingly one could imagine an algorithm with two independent conjugate momenta, maybe living in the perpendicular plane ( $\phi \cdot \pi = 0$ ). However, changing the constraint from the field  $\phi$  to the momenta is not very appealing (and, from the practical side, one would need to worry about *two* constraints in the numerical integration). A different approach, the use of spherical coordinates, has the drawback of a non-planar integration measure. Our very simple algorithm avoids constraints and non-planar measures, by introducing *three* conjugate momenta per spin.

We shall start from an analogy with the dynamics of a particle living in the sphere, a potential ( $V$ ) acting on it. The Hamiltonian is

$$H^{\text{sphere}} = \frac{\mathbf{L}^2}{2} + V(\phi). \quad (40)$$

Here  $\mathbf{L}$  is the angular momentum,  $\phi \times \dot{\phi}$ . The equations of motion can now be obtained from the Poisson Bracket [37] with the hamiltonian (40):

$$\dot{\phi} = \mathbf{L} \times \phi, \quad \dot{\mathbf{L}} = -\phi \times \frac{\delta V}{\delta \phi}. \quad (41)$$

In this expression  $\frac{\delta V}{\delta \phi}$  stands for  $\left( \frac{\delta V}{\delta \phi_1}, \frac{\delta V}{\delta \phi_2}, \frac{\delta V}{\delta \phi_3} \right)$ .

This formalism is still inconvenient for us, because the constraint  $\boldsymbol{\phi} \cdot \mathbf{L} = 0$  complicates the generation of random momenta according to a Gaussian distribution. However, the following simple facts can be straightforwardly established from the equations (41):

**I.** Both  $\phi^2$  and  $\boldsymbol{\phi} \cdot \mathbf{L}$  are conserved through the time evolution. If the initial condition verifies the constraints  $\phi^2 = 1$ ,  $\boldsymbol{\phi} \cdot \mathbf{L} = 0$ , this will not be spoiled by the dynamics.

**II.** The dynamics is time-reversible.

**III.** Although the  $L_i$  cannot be all canonical variables [37], the ‘‘Liouville’’ measure,  $D\boldsymbol{\phi} D\mathbf{L}(= d\phi_1 d\phi_2 d\phi_3 dL_1 dL_2 dL_3)$ , is left invariant by the time-evolution.

**IV.** The Hamiltonian is a constant of the motion.

Now let us forget about the constraint  $\boldsymbol{\phi} \cdot \mathbf{L} = 0$ , *i.e.* we introduce a new field  $\mathbf{P}$  which can have a ‘‘radial component’’ (it is no longer an angular momentum), but we keep the Eqs. of motion (41). Obviously, statements **I–IV** will still hold. Whether a symplectic structure is hidden under this new dynamical system is unclear, but also irrelevant (properties **II** and **III** are the essential ones for HMC to be a correct algorithm [36]).

So, we introduce three momenta per spin,  $\mathbf{P} = (P_1, P_2, P_3)$ , and write down the Hamiltonian

$$H = \sum_x \frac{\mathbf{P}^2}{2} + S_B(\boldsymbol{\phi}). \quad (42)$$

Equations of motion respecting properties **I–IV** are easily generalized:

$$\dot{\boldsymbol{\phi}}_{(x,\tau)} = \mathbf{P}_{(x,\tau)} \times \boldsymbol{\phi}_{(x,\tau)}, \quad \dot{\mathbf{P}}_{(x,\tau)} = -\boldsymbol{\phi}_{(x,\tau)} \times \frac{\delta S_B}{\delta \boldsymbol{\phi}_{(x,\tau)}}. \quad (43)$$

As expected, the evolution equations for the  $S^2$  fields  $\boldsymbol{\phi}$  take the form of (infinitesimal) rotations, while the conjugate momenta can be considered as living in the Lie Algebra of  $\text{SO}(3)$ . The discretized leap-frog form of these equations is therefore naturally formulated in terms of finite  $\text{SO}(3)$  rotations,

$$\boldsymbol{\phi}_x(n\Delta\tau + \Delta\tau) = \exp[\Delta\tau \mathbf{P}_x((n + \frac{1}{2})\Delta\tau) \cdot \mathbf{J}] \boldsymbol{\phi}_x(n\Delta\tau), \quad (44)$$

$$\mathbf{P}_x((n + \frac{1}{2})\Delta\tau) = \mathbf{P}_x((n - \frac{1}{2})\Delta\tau) - \boldsymbol{\phi}_{(x,n\Delta\tau)} \times \frac{\delta S_B}{\delta \boldsymbol{\phi}_{(x,n\Delta\tau)}} \Delta\tau, \quad (45)$$

where  $\mathbf{J}$  are the  $3 \times 3$  generators of  $\text{SO}(3)$ , satisfying

$$(\exp[\boldsymbol{\theta} \mathbf{n} \cdot \mathbf{J}])_{ij} = \delta_{ij} \cos \theta + n_i n_j (1 - \cos \theta) - \epsilon_{ijk} n_k \sin \theta \quad (46)$$

for unit vectors  $\mathbf{n}$ . Again, the length constraint on the  $\boldsymbol{\phi}$  fields is preserved by construction.

This final result is reminiscent of the elegant solution for models with variables belonging to a Lie group and conjugate momenta in the group algebra (or vice versa) [35].

In our case,  $S_{B \text{ quenched}} = -k \sum_{n,\mu} \boldsymbol{\phi}_n \cdot \boldsymbol{\phi}_{n+\hat{\mu}}$ , so the HMC algorithm can now be implemented in a straightforward manner. To test the algorithm, we have simulated the  $\text{O}(3)$  model on an  $8^3$  lattice at  $k = 0.693 \approx k_c$  [38] with our HMC algorithm and with Wolff’s single-cluster embedding algorithm [39]. Let us first define the measured observables, and then compare them.

In this work we have only measured bosonic observables, as our sole objective was the numerical determination of the phase diagram. We have constructed our observables in

Table 1: Values for several observables in the quenched model (3) on an  $8^3$  lattice at  $k = 0.693 \approx k_c$ , obtained with our implementation of HMC and with Wolff’s single cluster algorithm [39].

Algorithm	$\langle E \rangle$	$\partial_k \langle E \rangle$	$\chi/V$	$\xi$	$B$
HMC	0.3505(5)	1.51(2)	0.1426(9)	4.47(2)	0.800(6)
Wolff	0.35061(13)	1.501(10)	0.1432(2)	4.486(9)	0.8031(18)

terms of the Fourier transform of the spin field:

$$\hat{m}(\mathbf{p}) = \frac{1}{V} \sum_{\mathbf{x}} \exp(-i\mathbf{p}\cdot\mathbf{x}) \phi_{\mathbf{x}}, \quad (47)$$

where  $V = L^3$  is the lattice volume.

We define the non-connected finite-volume susceptibilities as

$$\chi = V \langle \hat{m}^2(0, 0, 0) \rangle, \quad \chi_s = V \langle \hat{m}^2(\pi, \pi, \pi) \rangle. \quad (48)$$

The subscript ‘s’ on  $\chi_s$  stands for ‘staggered’, and this term is used to label quantities which are taken with a weight  $-1$  for the odd lattice sites, corresponding to momentum  $(\pi, \pi, \pi)$ . Notice that  $\chi/V$  is a pseudo order parameter, which should be of order one in a ferromagnetically broken phase, and of order  $1/V$  in a paramagnetic or antiferromagnetic phase (and similarly for  $\chi_s/V$ ).

Another quantity of interest is the Binder cumulant

$$B = \frac{5}{2} - \frac{3}{2} \frac{\langle (\hat{m}^2(0, 0, 0))^2 \rangle}{\langle \hat{m}^2(0, 0, 0) \rangle^2}, \quad (49)$$

with an analogous definition for the staggered variant  $B_s$ .

One expects  $B = 1$  in the FM phase, where  $\chi/V$  is non-vanishing in the thermodynamic limit, while it should be of order  $1/V$  in the PM phase, far from the phase transition.

For the correlation length, we use a definition which is easy to measure and gives accurate results:

$$\xi = \left( \frac{\chi/F - 1}{4 \sin^2(\pi/L)} \right)^{1/2}, \quad (50)$$

where  $F$  is the squared Fourier transform at minimal non-zero momentum,

$$F = \frac{V}{3} \left( \langle |\hat{m}(2\pi/L, 0, 0)|^2 \rangle + \text{permutations} \right). \quad (51)$$

Again, the generalization to staggered quantities is straightforward. Another kind of observable, needed for the standard extrapolation method [42], is the normalized nearest-neighbour energy

$$E = \frac{1}{3V} \sum_{x,\mu} \langle \phi_x \cdot \phi_{x+\hat{\mu}} \rangle = \frac{\partial}{\partial k} \ln Z. \quad (52)$$

We also measure its fluctuation, given by

$$3V \left( \langle E^2 \rangle - \langle E \rangle^2 \right) = \frac{\partial}{\partial k} \langle E \rangle. \quad (53)$$

In Table 1 we compare the values obtained for these observables, using our HMC algorithm and the single-cluster algorithm. We find excellent agreement. Of course the efficiency of our implementation of HMC is not competitive with a cluster method in the O(3) non-linear  $\sigma$ -model. But it could be useful in other models where cluster methods are not effective in reducing the dynamical critical exponent  $z$  (for instance, when some kind of frustration is present [40]), while HMC is expected to yield  $z = 1$  for any bosonic model.

## 4.2 The HMC algorithm for the full theory

The only restriction imposed on HMC is that the fermion bilinear in the action should be given in terms of a positive definite matrix. This will be the case if we consider two identical fermion families ( $N_f = 2$ ) as is usually done in lattice gauge theories. After integrating them out we obtain  $(\det \hat{M})^2 = \det(\hat{M}^\dagger \hat{M})$ , where  $\hat{M}$  is the fermion matrix for a single fermion family. As we are mainly interested in the strong spin-fermion coupling region, it makes sense to perform the following manipulation:

$$\det \hat{M} = \det(Y + K) = y^{4V} \det(1 + Y^{-1}K) \quad (54)$$

(cf. Eqs. (30,31)). The constant factor  $y^{4V}$  can be dropped, and we define  $M = 1 + Y^{-1}K$ .

Next, one re-exponentiates the (inverse) fermion matrix by introducing the so-called *pseudo-fermions*  $z_x$ , which are complex four-component c-number fields. The partition function is then

$$Z = \int D\phi D\bar{z} Dz \exp\left(-S_B - \bar{z}(M^\dagger M)^{-1}z\right). \quad (55)$$

For further details we refer to Ref. [36].

Now the HMC Hamiltonian becomes

$$H = \sum_x \frac{1}{2} \mathbf{P}_x^2 - k \sum_{x,\mu} \phi_x \cdot \phi_{x+\mu} + z^\dagger (M^\dagger M)^{-1} z, \quad (56)$$

and the time reversible, constraint and energy preserving equations of motion are

$$\begin{aligned} \dot{\phi}_{(x,\tau)} &= \mathbf{P}_{(x,\tau)} \times \phi_{(x,\tau)}, \\ \dot{\mathbf{P}}_{(x,\tau)} &= -k \sum_{\mu} \left( \phi_{(x+\mu,\tau)} + \phi_{(x-\mu,\tau)} \right) \times \phi_{(x,\tau)} \\ &\quad - z^\dagger (M^\dagger M)^{-1} \left[ \left( \frac{\delta M^\dagger}{\delta \phi_{(x,\tau)}} \times \phi_{(x,\tau)} \right) M + h.c. \right] (M^\dagger M)^{-1} z. \end{aligned} \quad (57)$$

For the inversion of the fermionic matrix, we have employed the conjugate gradient algorithm. To formulate the stopping criterium, let us define  $h = (M^\dagger M)^{-1} z$ ,  $h_n$  being the  $n^{\text{th}}$  trial solution. We continued the conjugate gradient iteration until

$$\frac{|(M^\dagger M) h_n - z|^2}{|h_n|^2} \leq R. \quad (58)$$

In the simulation, we need the inverse matrix both for the leap-frog and for the Metropolis accept-reject step. It is clear that  $R$  does not need to be the same in both cases. For the Metropolis step, lack of accuracy in the inversion will bias the simulation. To control this, we have checked that the Creutz parameter  $\langle \exp(-\Delta H) \rangle$  equals 1 within errors. In some regions of parameter space  $R$  values as small as  $10^{-25}$  were needed. The essential requirement on the leap-frog is full reversibility in the numerical integration of the equations of motion (up to the numerical precision reachable with 64-bit floating point arithmetic). As first noticed in ref. [41], this has no relation with  $R$  if the seed for the conjugate-gradient algorithm is chosen to depend on the *actual* configuration only ( $h_0 = z$ , for instance). However, if  $R$  is too large, the numerical integration will produce large changes in the Hamiltonian, and the Metropolis acceptance will be poor. We have found that  $R = 10^{-7}$  during the leap-frog steps allows for a 50% acceptance.

In a first implementation of a new MC algorithm, some consistency checks are extremely useful. In addition, there are three parameters to be adjusted for optimal performance,  $N, \tau$  and  $R$ . We have carried out the following tests:

1. We have explicitly checked reversibility of the leap-frog algorithm.
2. We have checked that  $\langle \exp(-\Delta H) \rangle = 1$  within errors.
3. The gaussian expectation values,  $\langle z^\dagger (M^\dagger M)^{-1} z \rangle = 4$  and  $\langle \mathbf{P}^2 \rangle = 3$  have been checked.
4. We have checked that  $\Delta H \propto (\Delta\tau)^2$  in the leap-frog integration, for constant trajectory length  $N\Delta\tau$ .

In addition, we compared simulation results for the full theory at  $(k, y)$ , with the output of a quenched simulation at the corresponding effective coupling value obtained in a large- $y$  expansion,

$$k^{\text{eff}} = k + \frac{2}{y^2} + O\left(\frac{1}{y^4}\right) \quad (59)$$

(cf. Eq. (34)). In table (2), we give the mean value of several operators as obtained on a  $4^3$  lattice at  $k = 0.693$ ,  $y = 10.0$  and in the quenched theory. The agreement is excellent. Notice that even if the shift in the effective coupling is only 3%, the effects of the dynamical fermions can be clearly measured as the observables change quite significantly at the critical point  $k_c = 0.693$ .

### 4.3 Phase Diagram

The phase diagram in fig. 1 was obtained on an  $8^3$  lattice. As there is no true phase transition on a finite lattice, a criterium is needed to locate the phase boundaries. We looked for the point where the relevant Binder cumulant equals the value  $B = 0.8$  it has at  $(k = \pm 0.693 \approx k_c, y = 0)$ . Since  $B = 1$  deep in the broken phase and  $B \propto 1/L^3$  in the symmetric one, this provides a clean quantitative criterium which yields a point definitely inside the critical region. The width of the critical region decreases as  $L^{-1/\nu}$ , therefore the systematic error in the critical coupling will be at most of order  $10^{-1}$ . However, since the Binder parameter is a universal quantity, which should stay constant along much of the

critical lines, the error rather goes as  $L^{-(\omega+1/\nu)}$  (*i.e.*  $\mathcal{O}(10^{-2})$ ). Thus, this systematic error is under control in the full theory as well. We used the Ferrenberg-Swendsen extrapolation method to determine the precise location of the points where  $B = 0.8$ .

The total simulation time was 16 days of the 32 Pentium Pro processor parallel computer RTNN based in Zaragoza. To allow for a correct thermalization, we discarded 100 integrated autocorrelation times of the relevant susceptibility. This may look utterly conservative, and the MC history indeed seems to stabilize long before that. However, not much is known about the *exponential* autocorrelation time of fermionic algorithms and one should be cautious.

As Eq. (54) shows, both at  $y = \infty$  and at  $y = 0$  we recover the non-linear  $\sigma$ -model with its well known paramagnetic, ferromagnetic and antiferromagnetic phases. At finite  $y$ , we expect these phases to extend into the  $(k,y)$  plane. In fact one can quite precisely anticipate the critical coupling from the strong coupling formula (59) and the quenched critical points  $k_c^{(y=\infty)} = \pm 0.693$ . Using the Ferrenberg-Swendsen extrapolation procedure, the phase transition lines can be determined down to  $y \approx 2.0$ . In fig. 2 the variation of the Binder cumulant and the susceptibility around the two critical couplings is shown for  $y = 2.0$ .

In the small- $y$  region, the effective action up to  $\mathcal{O}(y^2)$  does not only renormalize  $k$ , but also introduces additional couplings, due to the non-locality of the matrix  $K^{-1}$  occurring in the weak-coupling expansion. Therefore, we do not have an estimate for  $k^{\text{eff}}$  as reliable as in the large- $y$  region (59), but we can nevertheless obtain an estimate for  $k_c(y)$  from the MF approximation. We have simulated at several values of the coupling  $k$ , for fixed  $y$ , until the corresponding Binder parameter crossed its critical value. A more accurate result for the critical point was later on obtained with the Ferrenberg-Swendsen extrapolation. In fig. 3, we have plotted the relevant Binder parameter and susceptibility for  $k$  values near the two critical couplings with  $y = 0.5$ .

In fig. 4 we show the variation of both order parameters and Binder cumulants when crossing the FM(S)-EM transition line at  $y = 1.15$ . We find a strong change in the staggered quantities, while the non-staggered ones show a smoother evolution. However, the non-staggered order parameter is much smaller than its staggered counterpart. This may indicate that, although the non-staggered sector is non-critical ( $B \sim 1$ ), it will eventually undergo a phase transition at lower  $k$ . A similar behaviour is found when traversing the AFM(W)-EM line at  $k = -1.6$  (see fig. 5), but now the non-staggered quantities show a

Table 2: Comparison of observables in the full theory (3) at  $(k = 0.693, y = 10.0)$  and in the quenched model both at the corresponding value of  $k^{\text{eff}}$  and at  $k_c = 0.693$ . We have 140,000 unquenched trajectories ( $N=10, \Delta\tau=0.3$ ) on a  $4^3$  lattice. The Metropolis acceptance rate was 65-70%, with an autocorrelation time of 3-4 trajectories.

Couplings	$\langle E \rangle$	$\partial_k \langle E \rangle$	$\chi/V$	$\xi$
$k=0.693, y=10.0$	0.4164(6)	1.134(6)	0.3111(7)	2.378(4)
$k=0.713, y=0$	0.41584(14)	1.130(4)	0.3108(2)	2.3779(18)
$k=0.693, y=0$	0.3928(3)	1.174(4)	0.2836(4)	2.214(2)

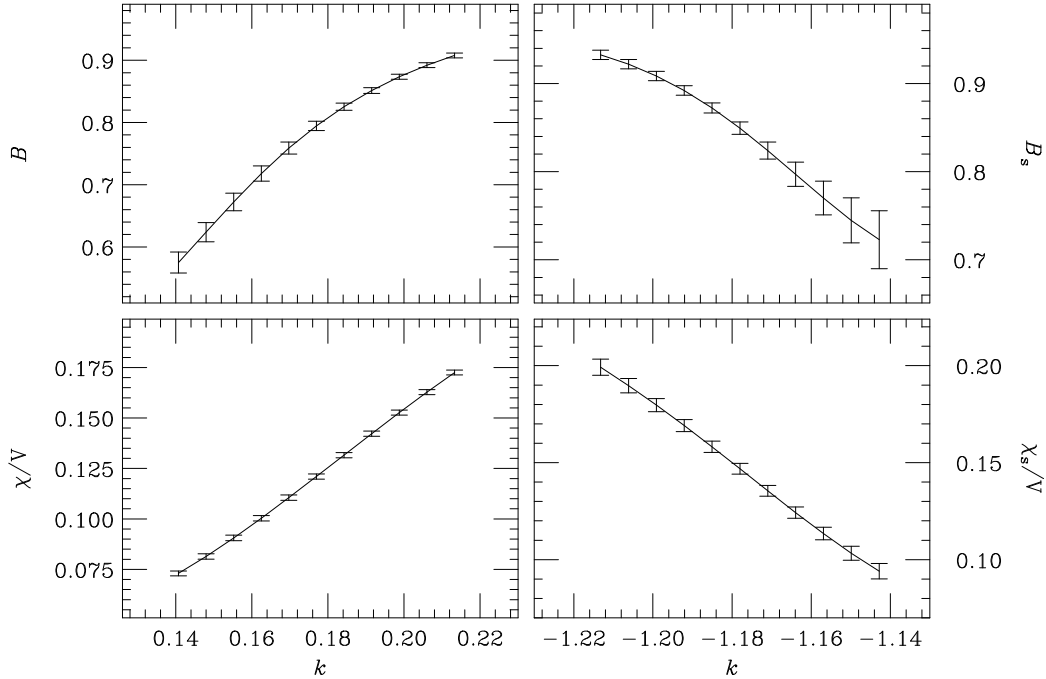


Figure 2: Binder cumulant (49) and non-connected susceptibility (48) as a function of  $k$ , around the two critical points at  $y = 2.0$ . For each critical point, only one simulation has been carried out. The other points are obtained with the Ferrenberg-Swendsen extrapolation method.

more pronounced signal. The detailed study of these transition lines (order of the phase transitions, critical exponents, etc.) requires a finite-size scaling analysis, which is left for future work. This study will be much easier if the transition line is crossed varying  $k$ , as we lack an analogue of the Ferrenberg-Swendsen extrapolation method for  $y$ .

## 5 Quasiparticle excitations at the MF level

In this section we explore the relevant excitations involving fermions, with emphasis on the strong-coupling region of our model. This will then enable us to discuss electronic properties.

The small- $y$  regime has been studied in relation with the mechanism by which leptons and quarks acquire their mass through symmetry breaking in the Electroweak sector of the Standard Model. Due to the weak coupling, one has essentially Fermi liquid behaviour, and there are no surprises. This situation will change dramatically when we consider the strong-coupling region, though.

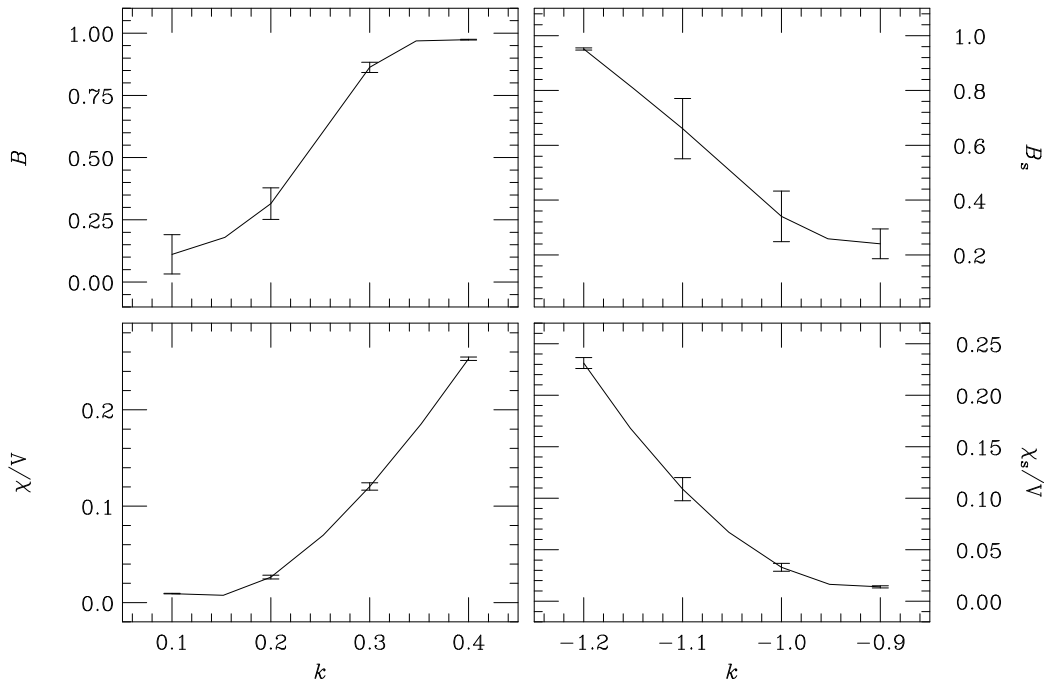


Figure 3: Binder cumulant (49) and non-connected susceptibility (48) as a function of  $k$ , around the two critical points at  $y = 0.5$ . The data points are from different simulations.

## 5.1 Fermionic excitations in the FM(S) and PMS phases

At very large  $y$ , it is natural to attempt a large- $y$  expansion. This can be achieved after carrying out the following change of variables:

$$\bar{\psi}' = \bar{\psi}, \quad (60)$$

$$\psi' = (\boldsymbol{\phi} \cdot \boldsymbol{\tau}) \psi. \quad (61)$$

Because of the constraint  $\boldsymbol{\phi}^2 = 1$  and the identity  $(\boldsymbol{\phi} \cdot \boldsymbol{\tau})^2 = \boldsymbol{\phi}^2 \mathbf{1}$ , this transformation has unit Jacobian and its inverse satisfies

$$\psi = (\boldsymbol{\phi} \cdot \boldsymbol{\tau}) \psi'. \quad (62)$$

In terms of the new variables (dropping the primes) the action takes the form

$$S = -k \sum_{x,\mu} \boldsymbol{\phi}_x \cdot \boldsymbol{\phi}_{x+\mu} + \sum_{x,y} \bar{\psi}_x (K_{xy} (\boldsymbol{\phi}_y \cdot \boldsymbol{\tau}) + y \delta_{xy}) \psi_y, \quad (63)$$

where the fermion kinetic term is the usual lattice kinetic Dirac operator, defined in Eq. (12). After a further rescaling of the  $\psi$  fields, the coupling  $y$  can be moved to the kinetic term, where it appears as  $1/y$ .

Note that this change of variables (60,61) was implicitly present in the MF calculations of the phase diagram in the strong-coupling region as well (cf. Eqs. (30,31)).

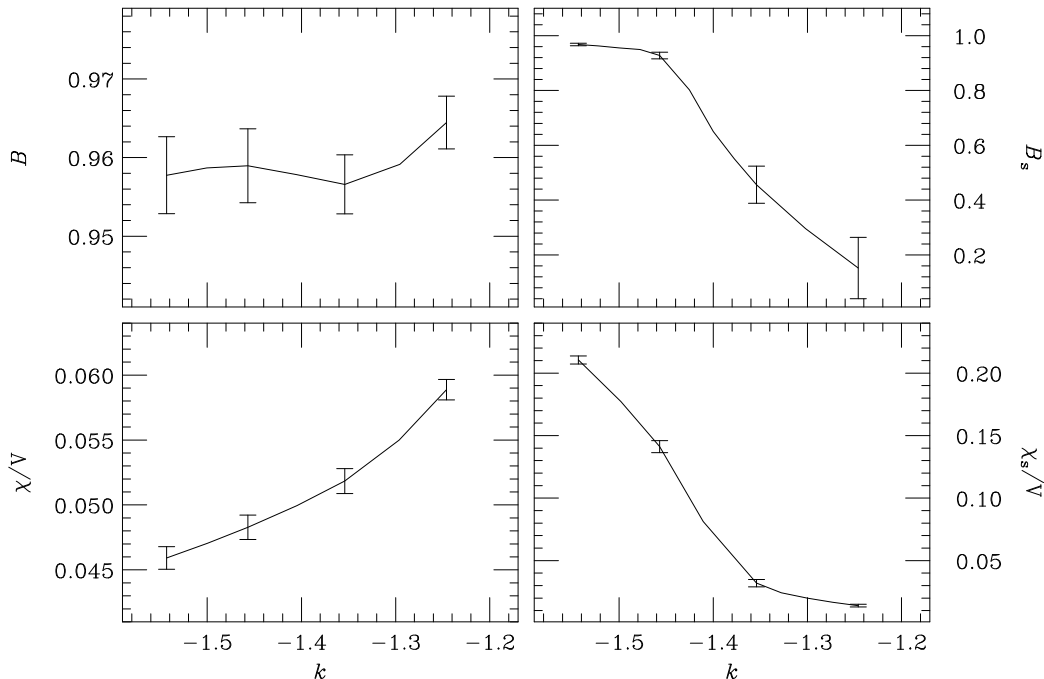


Figure 4: Binder cumulants and susceptibilities when crossing the FM(S)-EM transition line at  $y = 1.15$ .

The fermion propagator  $\langle \psi_x \bar{\psi}_y \rangle$  is given by the expectation value of the inverse fermion matrix, which in a large- $y$  expansion becomes

$$\langle \psi_x \bar{\psi}_y \rangle = \langle M_{xy}^{-1} \rangle = \left\langle \frac{1}{y} \left( 1 - \frac{1}{y} K(\phi \cdot \tau) + \frac{1}{y^2} K(\phi \cdot \tau) K(\phi \cdot \tau) - \dots \right)_{xy} \right\rangle. \quad (64)$$

This can be viewed as a sum over paths of increasing length connecting  $x$  and  $y$  (recall that  $K$  is a nearest-neighbour matrix).

In the FM(S) phase, there is a non-zero magnetization  $v = |\langle \phi \rangle|$ . Expectation values of products of  $\phi$  fields on different sites are replaced by the appropriate powers of  $v$ . Corrections to this approximation as well as contributions from paths visiting a given site more than once are of higher order in  $1/d$  and are ignored at the MF level. The series (64) can thus be resummed and one finds a propagator

$$\langle \psi \bar{\psi} \rangle_{FM(S)} = \frac{1/v}{K + y/v} \quad (65)$$

which is that of a fermion with a mass  $y/v$ . Note that, since  $v < 1$ , this is a huge mass if  $y$  is large. The propagator for the original fermion, before the change of variables (60,61), corresponds to the same physical particle; the only difference is in the wave function renormalization.

In the PM(S) phase,  $v = 0$ , so at the MF level the fermion would be infinitely massive, or in other words, non-propagating. Beyond this naive MF level, however, a large but

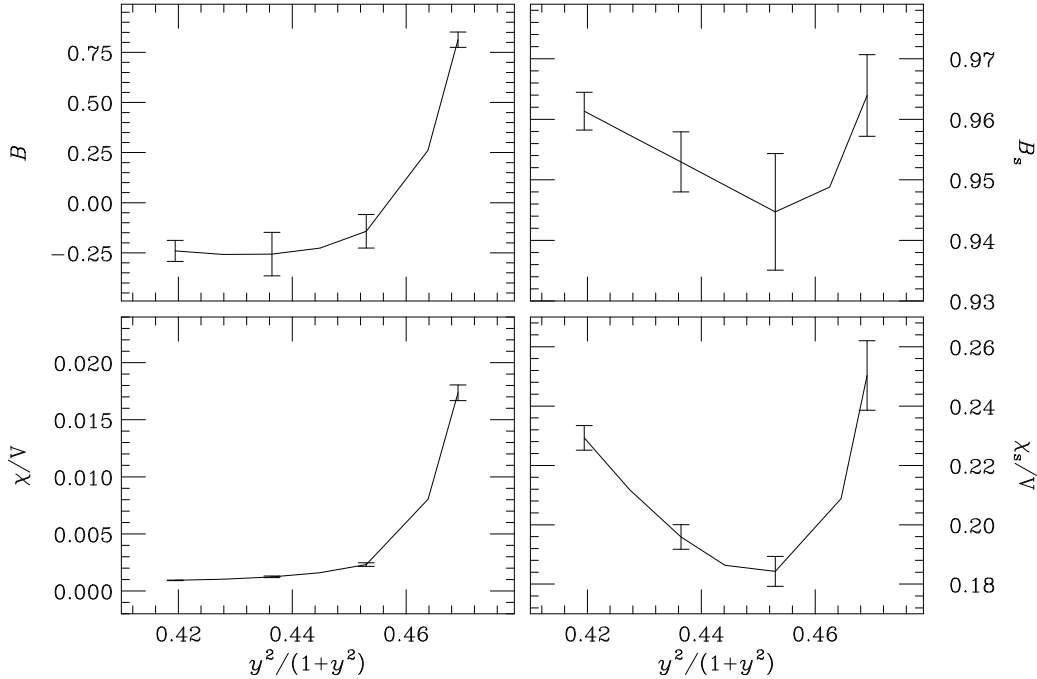


Figure 5: Binder cumulants and susceptibilities when crossing the AFM(W)-EM transition line at  $k = -1.6$ .

finite mass will be found. This is due to the next-to-leading contributions to the series (64). The dominant terms are now those involving the expectation value for the nearest-neighbour energy  $z^2 \equiv \langle \phi_x \cdot \phi_{x+\hat{\mu}} \rangle$ , which is of order  $1/2d$  and therefore absent at the MF level. The resummation of contributions in (64) now leads to a fermion propagator with a mass  $y/z$ , which is even larger than the mass of the fermion in the FM(S) phase.

The conclusion of this analysis, which is similar to that in (chiral) Yukawa models in the Electroweak theory [44], is that the elementary fermion excitations in the large- $y$  region are very heavy (hence essentially non-propagating), and therefore play no role in the spectrum of light excitations. This holds even stronger in the PMS phase than in the FM(S) phase.

## 5.2 Fermionic excitations in the AFM(S) phase

Here our point of departure is again the form of the action (63), which is tailored for studying the large- $y$  behaviour. In the AFM(S) phase, we have a staggered expectation value for the  $\phi$  field at the MF level, which can be taken in the 3-direction,

$$\phi_x = \epsilon_x v \begin{pmatrix} 0 \\ 0 \\ 1 \end{pmatrix} \quad (66)$$

(with  $\epsilon_x = (-1)^{x_1+x_2+x_3}$ ). Hence

$$(\phi_x \cdot \tau) \psi_x = \begin{pmatrix} v \epsilon_x \psi_x^{(1)} \\ -v \epsilon_x \psi_x^{(2)} \end{pmatrix}, \quad (67)$$

where  $\psi_x^{(i)}$ ,  $i = 1, 2$  labels the two *flavours* in  $\psi_x$ . So after the change of variables (60,61) the kinetic operator in (63) is still diagonal in flavour. The only effect of the new variables is to change the lattice Dirac operator from (12) to

$$v \epsilon_y \tau_3 K_{xy}.$$

Due to this diagonal structure in flavour space, we can concentrate on one flavour, say  $\psi^{(1)}$ ; the other flavour is obtained by taking  $-v$  instead of  $v$ . In Fourier space, the kinetic term for  $\psi^{(1)}$  is given by

$$-i v \text{s\!i\!n} p \delta_{p,q\pm\pi}, \quad (68)$$

where

$$\text{s\!i\!n} p = \sum_{\mu} \sigma_{\mu} \sin p_{\mu}, \quad (69)$$

$$\delta_{p,q\pm\pi} = \prod_{\mu} \delta_{p_{\mu},q_{\mu}\pm\pi \bmod 2\pi}. \quad (70)$$

So we obtain for the inverse of the MF propagator in the AFM(S) phase,

$$M_{p,q} = -i v \text{s\!i\!n} p \delta_{p,q\pm\pi} + y \delta_{p,q}, \quad (71)$$

or, in matrix notation for the subspace of the modes coupled in Eq. (71),  $p$  and  $p\pm(\pi, \pi, \pi)$ ,

$$M_{p,p\pm(\pi,\pi,\pi)} = \begin{pmatrix} y & -i v \text{s\!i\!n} p \\ i v \text{s\!i\!n} p & y \end{pmatrix}. \quad (72)$$

To find the quasiparticle excitations in the AFM(S) phase we diagonalize the fermionic part of the action (72). One obtains

$$S = \int_p \bar{\psi}(p) (y - v \text{s\!i\!n} p) \psi(p), \quad (73)$$

where

$$\psi(p) = \frac{1}{\sqrt{2}} \left[ \psi^{(1)}(p) + i \psi^{(1)}(p + \pi) \right],$$

or, in *position* space,

$$\psi_x = \frac{1}{\sqrt{2}} \left[ \psi_x^{(1)} + i \epsilon_x \psi_x^{(1)} \right].$$

The momentum space propagator corresponding to (73) is thus

$$S(p) = \frac{1}{y - v \text{s\!i\!n} p} = \frac{y + v \text{s\!i\!n} p}{y^2 - v^2 \sum_{\lambda} \sin^2 p_{\lambda}}. \quad (74)$$

Since we are working in imaginary time, one would expect quasiparticle poles in  $S(p)$  to appear at negative values of  $p^2$ . The unusual relative minus sign in the denominator (74) therefore does not seem to allow for a quasiparticle interpretation, at first sight.

However, (74) suggests the possibility of light excitations with a relativistic dispersion relation around spatial momenta  $(\pm\frac{\pi}{2}, \pm\frac{\pi}{2})$ . To see this, consider the denominator in Eq. (74) for small  $k_\mu = p_\mu \pm \pi/2$ :

$$y^2 - v^2 \sum_{\lambda} \sin^2 p_{\lambda} = (y^2 - v^2 d) + v^2 \sum_{\lambda} k_{\lambda}^2 + \mathcal{O}(k^4), \quad (75)$$

where  $d = 3$  is the space-time dimension. As long as we are at large enough  $y$ , such that  $y^2 > dv^2$  (recall  $v^2 < 1$ ), this dispersion relation corresponds to a relativistic excitation with  $m^2 = (y^2 - dv^2)/v^2$ , in this naive MF calculation. Several comments are in order:

1. For  $v=0$ , we recover the MF result for the PMS phase: the kinetic term in (75) is suppressed.
2. At the MF level, only for  $(y^2 - dv^2)$  small enough compared to  $v^2$  these fermionic excitations,  $(\boldsymbol{\tau} \cdot \boldsymbol{\phi}) \psi$ , can propagate easily. Since  $v^2 < 1$ , this can only happen for  $y^2$  not too large. Whether or not this situation will arise depends on the precise phenomenological relation between  $x$  and  $(y, k)$ , which is likely to be dopant-dependent (see section 2.2).
3. These would-be excitations are characteristic of the AFM(S) phase. Let us recall that in the PMS phase no *light* fermionic excitations have been identified at the MF level. In any case, in the SC phase of our model *we are not in an AFM background*. Therefore no momentum-space rotation will be needed to interpret the fermionic excitations and no hole-pockets around  $(\pm\pi/2, \pm\pi/2)$  are expected in the SC phase [18].
4. We need to fix the scale in some way, as done for instance in [7], to estimate by means of a MC calculation the masses of all possible excitations of our model.

### 5.3 Light bound states in the PMS phase

We have seen above that the fermionic excitations in the PMS phase are very heavy. We will now show that there are bound states of elementary fermions, however, which are light. This is done by means of a MF calculation of the double-chain type [43]. These pairs will be the electron or hole pairs responsible for the superconductivity, as we will discuss in Sect. 6.

Consider the propagator for a fermion pair  $\psi_x \psi_x$ ,

$$\langle \psi_{x,i}^{\alpha} \psi_{x,j}^{\beta} \bar{\psi}_{y,k}^{\lambda} \bar{\psi}_{y,l}^{\rho} \rangle = \langle M_{x,\beta,j;y,\lambda,k}^{-1} M_{x,\alpha,i;y,\rho,l}^{-1} \rangle - \langle M_{x,\alpha,i;y,\lambda,k}^{-1} M_{x,\beta,j;y,\rho,l}^{-1} \rangle. \quad (76)$$

Here  $M^{-1}$  is the single-fermion propagator,  $\alpha, \beta, \lambda, \rho$  are Dirac indices, and  $i, j, k, l$  are flavour indices. Thus, this propagator is really a  $16 \times 16$  matrix. For the moment we keep all these indices as they are; later on we will discuss how pairs of them decompose into quantum numbers for the composite state.

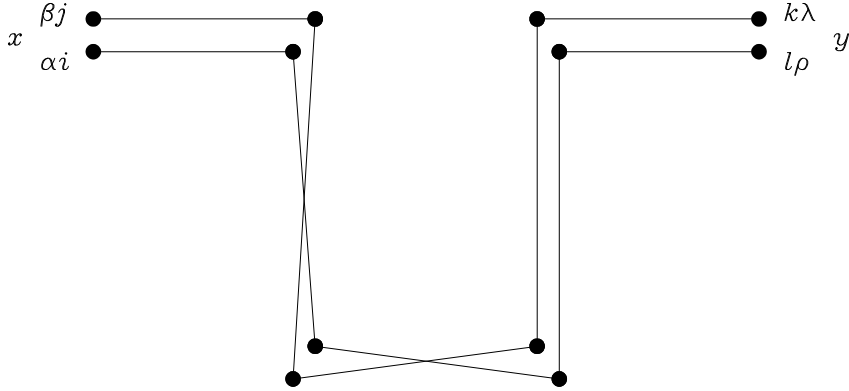


Figure 6: A typical double-chain diagram, connecting sites  $x$  and  $y$ . The chains are parallel in position space.

Let us concentrate on the first  $\langle M^{-1}M^{-1} \rangle$  term in Eq. (76). Using the  $1/y$  expansion of  $M^{-1}$  as before, we find the series

$$\langle M_{x,\beta,j;y,\lambda,k}^{-1} M_{x,\alpha,i;y,\rho,l}^{-1} \rangle = \sum_{N,N'=0}^{\infty} \left\langle \left[ \frac{\phi}{y} \left( K \frac{\phi}{y} \right)^N \right]_{x,\beta,j;y,\lambda,k} \left[ \frac{\phi}{y} \left( K \frac{\phi}{y} \right)^{N'} \right]_{x,\alpha,i;y,\rho,l} \right\rangle, \quad (77)$$

where we have written  $\phi$  as a shorthand for  $(\phi \cdot \tau)$ . It is clear that only terms with  $N + N'$  even survive in a paramagnetic phase, due to the  $\phi \rightarrow -\phi$  symmetry, thus a factor  $(-1)^{N+N'}$  has been dropped. Since the matrix  $K$  connects nearest-neighbour sites only, each term in this series can be seen to represent a product of two paths (chains) of lengths  $N$  and  $N'$  respectively, connecting site  $x$  with site  $y$  (so, if the “distance” between  $x$  and  $y$  is even(odd), both  $N$  and  $N'$  will be even(odd)).

We will attempt to sum the complete series, to leading order in  $1/d$ , where  $d = 1+2 = 3$  is the euclidean space-time dimension. For this, we need the spin-spin propagator, which in this approximation is extremely short ranged

$$\langle \phi_x^a \phi_x^b \rangle = \frac{1}{3} \delta^{ab}. \quad (78)$$

Expectation values of the type  $\langle \phi_x \cdot \phi_{x+\hat{\mu}} \rangle$  are of order  $1/d$ , and others are suppressed even stronger. Thus, assuming (78), we observe that any term in the series which contains  $\phi_x$  for a given site  $x$  only once or an odd number of times will vanish due to  $\langle \phi \rangle = 0$ . When the site is visited twice, it follows from  $\phi^2 = 1$  that the contribution from the  $\phi$  fields is proportional to  $\frac{1}{3} \delta^{ab}$ . Thus each site along the chains connecting  $x$  and  $y$  must be visited an even number of times. One class of diagrams fulfilling this requirement consists of the so-called ‘double-chain’ diagrams, where the propagation of both fermions between  $x$  and  $y$  follows the same path in position space (see figure 6). As was convincingly argued in Ref. [43], this class saturates the dominant diagrams in the  $1/d$  expansion. Indeed, one can easily check by concrete examples, how deviations from double-chain behaviour induce additional powers of  $1/d$ . We shall also assume that these double chains are self-avoiding (this is allowed at first order in  $1/d$ ).

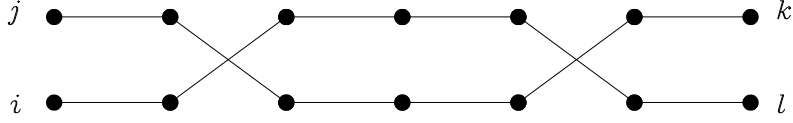


Figure 7: A matrix-product term contributing to the flavour structure.

Our task is thus to sum up all double chain diagrams connecting  $x$  and  $y$ . Let us first consider the flavour structure. Using (78) one finds that

$$\langle (\phi_x \cdot \tau)_{jk} (\phi_x \cdot \tau)_{il} \rangle = \frac{1}{3} \sum_a \tau_{jk}^a \tau_{il}^a = \frac{1}{3} (-\delta_{jk} \delta_{il} + 2\delta_{jl} \delta_{ik}). \quad (79)$$

From this and from the ultra-local correlations we are considering (cf. Eq. (78)), it follows that the product of  $2(N+1)$  factors of  $(\phi \cdot \tau)$  along a double chain of length  $N$  visiting the points  $x = x_0, x_1, \dots, y = x_N$  (cf. Eq. (77)) is

$$\left\langle \left[ \prod_{n=0}^N (\phi_{x_n} \cdot \tau) \right]_{x,j;y,k} \left[ \prod_{n'=0}^N (\phi_{x_{n'}} \cdot \tau) \right]_{x,i;y,l} \right\rangle = P \delta_{jk} \delta_{il} + Q \delta_{jl} \delta_{ik}. \quad (80)$$

To calculate  $P$  and  $Q$ , it is convenient to represent the general term contributing to the above matrix product as in figure 7. A graph contributing to  $\delta_{jk} \delta_{il}$  will have an even number of crossings, while diagrams contributing to  $\delta_{jl} \delta_{ik}$  jump an odd number of times. Each crossing contributes a factor  $\frac{2}{3}$ , while non-crossings yield factors  $-\frac{1}{3}$  (cf. Eq. (79)). Now,  $P$  and  $Q$  can be easily obtained using binomial summation:

$$\begin{aligned} & \left\langle \left[ \prod_{n=0}^N (\phi_{x_n} \cdot \tau) \right]_{x,j;y,k} \left[ \prod_{n'=0}^N (\phi_{x_{n'}} \cdot \tau) \right]_{x,i;y,l} \right\rangle \\ &= \left( \frac{1}{3} \right)^N \frac{1}{2} (\delta_{jk} \delta_{il} + \delta_{jl} \delta_{ik}) + (-1)^N \frac{1}{2} (\delta_{jk} \delta_{il} - \delta_{jl} \delta_{ik}), \end{aligned} \quad (81)$$

where we have separated in a term symmetric under  $(ji) \leftrightarrow (ij)$  and an antisymmetric one (this will be needed for separating the contribution to different quantum numbers). It is remarkable that the flavour contribution only depends on the double-chain length, but not on its shape. This allows for a total factorization between flavour and Dirac indices.

Next, consider the Dirac structure. One gets products of matrices

$$K_{x_n x_{n+1}}^{\mu_n} K_{x_n x_{n+1}}^{\mu_{n+1}} \sigma_{\beta_n \lambda_n}^{\mu_n} \sigma_{\beta_{n+1} \lambda_{n+1}}^{\mu_{n+1}}, \quad (82)$$

along the double chain, where

$$K_{xy}^{\mu} = \frac{1}{2} (\delta_{y, x+\hat{\mu}} - \delta_{y, x-\hat{\mu}}). \quad (83)$$

One readily finds that

$$A_{xy}^{\mu} \equiv 4 K_{xy}^{\mu} K_{xy}^{\mu} = (\delta_{y, x+\hat{\mu}} + \delta_{y, x-\hat{\mu}}). \quad (84)$$

Thus, we need to calculate

$$\sum_{\{\mu_n\}} \left[ \prod_n \frac{1}{4} A^{\mu_n} \sigma^{\mu_n} \otimes \sigma^{\mu_n} \right]_{x,\beta,\alpha;y,\lambda,\rho}, \quad (85)$$

where the sum is extended to all the lattice paths (denoted by  $\{\mu_n\}$ ) of-length  $N$  connecting  $x$  and  $y$ . Now, we can extend the sum to *all* length- $N$  lattice paths starting at  $x$ , because paths not connecting  $x$  to  $y$  will contribute a zero  $xy$  entry. This can be also understood by realizing that once the chain has arrived at  $x_i$ , there are  $2d$  possible directions to continue the chain. These are added up by summing Eq. (82) over  $\mu$ . At the next site, we do the same for the next step along the chain. The contributions of all double chains are therefore added up when we take the product of these  $\mu$ -sums along the chain. Corrections due to backtracking ( $2d \rightarrow 2d - 1$ ) are down by  $1/d$ .

So we need to calculate powers of the matrix

$$\frac{1}{4} \sum_{\mu} A^{\mu} \sigma^{\mu} \otimes \sigma^{\mu}. \quad (86)$$

One way to do that is to write it out explicitly as a  $4 \times 4$  matrix in the space spanned by the vectors  $(\beta, \lambda) = (1,1), (2,2), (1,2)$  and  $(2,1)$ , in that order. One finds that it equals

$$\frac{1}{4} \begin{pmatrix} A^3 & A^1 - A^2 & 0 & 0 \\ A^1 - A^2 & A^3 & 0 & 0 \\ 0 & 0 & -A^3 & A^1 + A^2 \\ 0 & 0 & A^1 + A^2 & -A^3 \end{pmatrix}. \quad (87)$$

It can be diagonalized in this  $4 \times 4$  space. The eigenvalues, up to the factor  $1/4$ , are found to be

$$\lambda^{\mu} = A - 2A^{\mu} \quad (\mu = 1, 2, 3), \quad (88)$$

$$\lambda^4 = -A, \quad (89)$$

where

$$A = \sum_{\mu=1}^3 A^{\mu} = \square + 2d, \quad (90)$$

and  $\square$  is the lattice discretization of the d'Alembertian  $\sum_{\mu} \partial_{\mu} \partial_{\mu}$ . The  $N^{\text{th}}$  power (see (85)) of the matrix (86) is now easy to calculate.

In order to collect the factors and sum up the contributions, let us go back to Eq. (76). We see that we need to antisymmetrize each term in  $\langle M^{-1} M^{-1} \rangle$  with respect to the simultaneous interchange of  $\alpha, i$  with  $\beta, j$ . This gives a sum of two terms, one symmetric in  $\alpha \leftrightarrow \beta$  and antisymmetric in  $i \leftrightarrow j$  (corresponding to a composite state which is a Dirac vector and a flavour singlet), and one vice versa (singlet in Dirac space, vector in flavour space). Note that Eq. (81) has already been written as a sum of symmetric and antisymmetric terms. The symmetric and antisymmetric parts of the Dirac structure correspond to Eqs. (88) and (89), respectively.

Collecting the various factors, we can carry out the geometric sum over  $N$  in Eq. (76) and we find the following propagators for the composite states:

- a Dirac vector – flavour singlet with propagator

$$\frac{8\delta^{\mu\nu}}{-\square + 2A^\mu - 4y^2 - 2d} \quad (91)$$

where  $a, b$  are the Dirac vector indices

- a Dirac singlet – flavour vector with propagator

$$\frac{-8\delta_{IJ}}{-\square - 12y^2 - 2d} \quad (92)$$

where  $I, J$  are the flavour vector indices.

These have the form of massive bosonic propagators, up to the following caveat (of course, higher order corrections in  $1/d$  may induce shifts in the precise location of the poles, as well as their residues).

The propagators in (91) contain the matrix  $2A^\mu$  in the denominator. However, this term must be ignored since it is sub-dominant in  $1/d$ , compared with the (lattice) d'Alembertian  $\square$ .

The numerator of the propagator (91) carries a delta function only, instead of the usual tensor structure  $\delta_{\mu\nu} - \partial_\mu\partial_\nu/m^2$ . This is also an artifact of the  $1/d$  approximation.

Notice also that the terms which would play the role of a mass squared in the denominators have an apparently wrong sign. However, it is easy to check that the composite field  $\epsilon_x\psi_x\psi_x$  (where  $\epsilon_x = (-1)^{\sum_\mu x^\mu}$  as usual) does lead to a massive Dirac singlet – flavour vector propagator with mass squared  $m_{(0,1)}^2 = 12y^2 - 2d = 12y^2 - 6$ . Similarly, one obtains a massive Dirac vector – flavour singlet with a mass squared  $m_{(1,0)}^2 = 4y^2 - 2d = 4y^2 - 6$ . We thus conclude that the right interpolating field is  $\epsilon_x\psi_x\psi_x$  [43] (one could equally well consider it as an excitation centered around spatial momentum  $(\pi, \pi)$ , though).

The conclusion is that we find massive bound states of fermions in the PMS phase. They are bound by the strong interactions with the spin waves. These composites are lighter than the elementary fermions in this phase, when  $y$  moves away from the value  $\infty$ . This means that they will be the dominant light excitations, and we will argue that they condense and lead to superconductivity in our model.

## 6 The $x$ - $T$ phase diagram of the cuprates

In this section we shall consider the application of the above results to the cuprates. Strictly speaking, our calculations only apply to the zero-temperature case. However, some conjectures can be made for the case of non-zero temperature, by means of very general thermodynamic considerations.

### 6.1 Physics at zero temperature

We will discuss how the copper oxide materials are described by our model, by following the ‘trajectory’ which they map out in the  $y, k$  phase diagram of our model as the doping fraction  $x$  is increased from zero all the way to the overdoped regime. Along the way,

various phases will be traversed, and the relevant light excitations present will be given their physical interpretation.

As we discussed earlier on, it is by now well established that the undoped material can be described by a point ( $k \lesssim k_c, y = \infty$ ) in the AFM(S) phase of the O(3) model to which our model reduces for  $y = \infty$ . The actual value of  $k$  is related to the spin stiffness and velocity; in the large- $S$  approximation  $k \propto S$  [7]. As the doping fraction  $x$  is increased, the carrier mobility increases which we have argued in section 2.2 to correspond to decreasing  $y$  in our model.

We have schematically indicated this ‘evolution’ of the cuprates with increasing doping by the line of arrows in Fig. 1. For illustrative purpose, let us assume (see our comment in section 2.2) a relation of the type  $x \sim C^2/(C^2 + y^2)$  for some constant  $C$  (in the case  $C = 1$  the horizontal axis in Fig. 1 would then correspond to  $1 - x$ ), but this is immaterial for the qualitative picture.

Note that we move in the direction of the PMS–AFM(S) transition line, so the AFM order will decrease. This is consistent with the experimentally observed reduction of AFM order upon doping.

At some point along our trajectory, still within the AFM(S) phase, the possible excitations at the  $(\pm\pi/2, \pm\pi/2)$  hole pockets (cf. Sect. 5.2) would become light and start to dominate.

When the doping is increased even more, we move into the PMS phase. As long as we remain close to the PMS–AFM(S) transition in this phase, short-range AFM correlations will still be present, although they are predicted to decrease as one moves deeper into this phase. The crucial point is that, as demonstrated in the MF calculation of Sect. 5.3, the only light excitations left now are the ‘‘PMS pairs’’, bosonic fermion bound states. Let us remark that a rich spectrum of excitations with different quantum numbers (not all of them identified in our MF calculation) should be expected. In our calculation, the flavour singlet (*i.e.* the physical spin-singlet) has turned out to be lighter than the triplet, which is encouraging. To investigate this fundamental point in more detail, a MC calculation has to be done.

At temperature  $T = 0$  these pairs will be Bose-Einstein (BE) condensed, as any other bosonic state would. This leads to superfluid behaviour for the pairs, and to superconductivity once electromagnetism is coupled into the model. Since a finite number  $\mathcal{O}(x_{c_1}/2)$  of them becomes available at the same time, at the point where we enter the PMS phase (corresponding to some critical doping  $x_{c_1}$ ), one expects a finite (*i.e.*, not infinitesimally small) critical temperature  $T_c = T_{\text{BE}}$  here.

Following the arrow line towards even smaller  $y$ , we leave the superconducting PMS phase at  $x_{c_2}$ . Thus we understand why *superconductivity only happens for a range of doping*. Again,  $T_c$  is expected to remain finite up to  $x_{c_2}$ . This may explain why  $T_c$  is experimentally observed to jump steeply at  $x_{c_{1,2}}$ ; however, we will discuss the possibility of even more unusual behaviour when we discuss the  $T \neq 0$  behaviour below.

Our model predicts a ferromagnetically ordered phase at  $T = 0$  in this intermediate- $y$  regime. The system traverses a region where one needs to go over from a description of the charge carriers in terms of the variables  $(\boldsymbol{\tau} \cdot \boldsymbol{\phi})\psi$  at large  $y$ , to a description in terms of the fields  $\psi$  appropriate for the small- $y$  Fermi-liquid regime. (There may be a kind of cross-over in this region.) In either description, propagation of the carriers is hampered by the effective mass induced by the FM spin waves.

At this point one may object that no FM behaviour has been observed experimentally in the overdoped regime. We note, however, that at some non-zero temperature (cf. Sect. 6.2), this phase will be replaced with a thermally disordered phase. Since the overdoped regime has not been explored in as much detail as the underdoped and superconducting regimes, in particular at very low temperatures, this may explain why no FM behaviour has been detected here.

For very large doping we reach the weak-coupling region with Fermi-liquid behaviour. We will end up in the PMW, AFM(W) phase or possibly remain in the FM(W) phase of our model. This will depend on the actual trajectory of the system with doping (see our comments in section 2.2, and recall that for large doping fraction the effective  $k$  parameter might also be influenced by it).

All these considerations illustrate how such widely varying behaviour in the cuprates, controlled by the doping fraction  $x$ , is reproduced by varying just one parameter in our simple two-parameter model. A point needing further investigation is the following. At strong coupling, one would expect a shift from commensurate to incommensurate AFM ordering, with increasing doping [45]. After integration out the fermion field in our model, frustrating couplings (of order  $1/y^4$  in the strong coupling expansion) are generated, which presumably lead to such a phenomenon. Our MC simulation, was done on a too small lattice to be able to resolve such an effect, and our MF is not reliable in this intermediate- $y$  region [33].

An interesting prediction of our model is that superconductivity is unlikely to occur in materials with spin  $S > 1/2$ . The reason is that the undoped model would correspond to a point  $k \ll k_c$  in the O(3) model ( $|k| \propto S$ , see ref. [7]), making it unlikely that the “evolution trajectory” pass through the PMS phase. In more physical terms, the larger  $|k|$  is in our model, the stiffer is the magnetic ordering and the less effective are the spin fluctuations needed to bind the fermions. For instance, upon doping the layered compounds  $\text{La}_{1-x}\text{Sr}_{1+x}\text{MnO}_4$ , which have localized  $S = 3/2$  spins (implying  $k \sim -2$  in the O(3) model) a disappearance of the antiferromagnetic phase and the subsequent emergence of an exotic magnetic phase (maybe a spin-glass phase) is observed [46], but no superconductivity appears. Essentially, the same thing happens for insulating nickelates  $\text{La}_{2-x}\text{Sr}_x\text{NiO}_4$ , for which the localized spin is  $S = 1$  [47].

## 6.2 Physics at non-zero temperature

What happens when the temperature is increased from zero? So far, we do not have any MF or MC results at non-zero temperature. However, by the following fairly general arguments we are led to conjecture Fig. 8 as a schematic sketch of the most general  $x$ - $T$  phase diagram suggested by our model.

First, let us discuss what happens with the superconducting phase when the temperature is increased. Consider a doping fraction  $x$  corresponding to a  $y$  value such that we are well inside the PMS phase, with superconductivity at  $T = 0$ . At a certain temperature,  $T_{\text{BE}}$ , the BE condensation will be undone, so the superconductivity disappears. We thus identify  $T_{\text{BE}}$  as the critical temperature  $T_c$ . Above  $T_c$  the fermions are still bound together in (uncondensed) light bosonic PMS pairs. One therefore expects “normal”, charge-2 conduction due to these pairs. This phase is sometimes called a “spin-gap” phase. As a matter of fact, the existence of such a phase is shared by any model in which superconductivity is

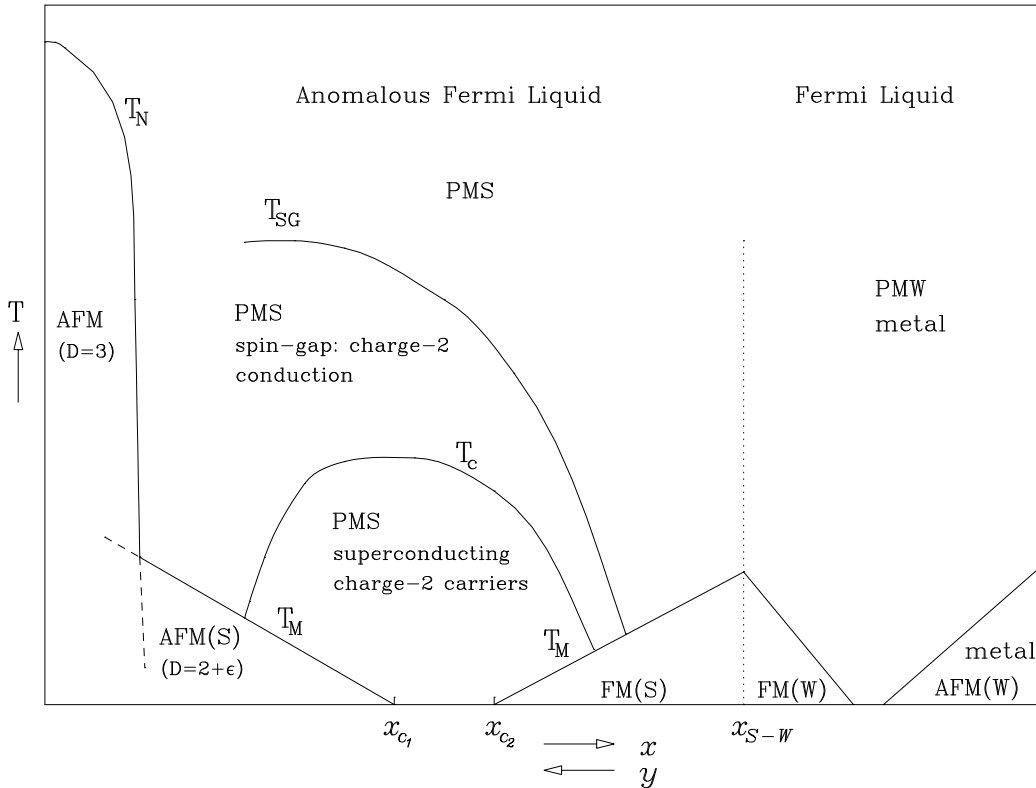


Figure 8: Sketch of the predicted phase structure in the  $x$ - $T$  plane. The dotted vertical line at  $x_{S-W}$  indicates a possible crossover.

triggered by the Bose-Einstein condensation of previously formed fermion-fermion bound states. Experimental evidence for such a mechanism is now available [3].

Above some spin-gap temperature,  $T_{SG}$ , the PMS pairs will be broken apart by thermal fluctuations. However, notice that the pair-breaking temperature for the first, isolated PMS-pair is lower than the temperatures needed to dissociate many of them, since the constituent fermions have to fill up states of increasing energy in the Fermi sea. Thus one expects  $T_{SG}$  to be characteristic of a cross-over rather than a well-defined phase transition. In this high-temperature phase, the only possible carriers would be fermions, but as we have already discussed, their kinetic term vanishes in the mean field approximation. (This perfectly insulating behaviour will receive corrections beyond the mean-field approximation, though.)

In the qualitative behaviour shown in Fig. 8, we have supposed that  $T_{SG}$  is always larger than  $T_{BE}$ . Depending on the variation of the mass and the binding energy of the bound state with doping, it could happen that the  $T_{SG}$  and  $T_{BE}$  critical lines join at some point. The actual situation regarding the full curves  $T_{SG}$  and  $T_{BE}$  would have to be investigated numerically in our model.

Further qualitative statements can be derived from the general thermodynamic argument that raising the temperature has the effect of increasing the magnetic disorder.

In the phase diagram of our model, Fig. 1, this means that the two PM phases expand in all directions, at the expense of the various magnetically ordered phases. One of the consequences could be a rash disappearance of the FM phase, which might explain why it has not been observed, as we briefly discussed in Sect. 6.1.

Another consequence is the intriguing possibility of re-entrant superconductivity for certain values of  $x$ , with superconductivity not starting at 0 K, but restricted to a temperature interval  $0 < T_M < T < T_c$ . To see this, consider  $x$  slightly smaller than  $x_{c_1}$ , corresponding to a point  $(y, k)$  in figure 1 inside the AFM(S) phase, very close to the transition to PMS. Let us assume the disorder due to the temperature has similar properties to the disorder coming from the dynamics (*i.e.* at zero temperature). Then the PMS phase will be enlarged and absorb the point  $(y, k)$ , implying superconductivity provided that we are still below  $T_{BE}$ . Similar re-entrant behaviour is expected for  $x$  slightly larger than  $x_{c_2}$ . In order to make quantitative predictions, an estimate of the mass and the binding energy of the PMS-pairs would be required. Some experimental evidence for reentrance has been found ten years ago [48] in YBaCuO, but it seems to have gone largely unnoticed. Further experiments are required to resolve this issue.

In fact, our model does not exclude the extreme case in which the superconducting phase is an island in the  $x$ - $T$  plane, completely detached from the  $T = 0$ -axis. However, this scenario seems hard to realize in real life, as it would require the  $T = 0$  evolution curve (the arrow line in Fig. 1) to pass underneath but very close to the PMS phase.

## 7 Conclusions

We have formulated and investigated a simple, spin-Dirac fermion field theory in 2+1 dimensions capable of explaining, at least qualitatively, a variety of experimental properties of the cuprate superconductors and their parent compounds as a function of doping fraction and temperature.

Our model provides a qualitative understanding of insulating, AFM behaviour at low doping, of high- $T_c$  superconductivity through the Bose-Einstein condensation of spin-disorder-bound charge pairs at intermediate doping, and of Fermi-liquid behaviour at large doping. In addition we have formulated several predictions, which may be amenable to experimental testing. In particular, we recall the possibility of reentrance (Sect. 6.2) and the statement that superconductivity is unlikely to occur in materials with  $S > 1/2$  (Sect. 6.1).

The model is constructed as an effective theory, using as ingredients only points 2,4 and 7 of the list of important experimental properties given in Sect. 1. As output, the model gives a reasonable explanation for the other points 1,3,5 and 6. We feel this is because we have been able to identify the essential degrees of freedom, and to pursue the consequences of the relevant symmetries in classifying their possible interactions.

If we succeed in computing, by means of Monte Carlo simulations, the masses and the binding energies present of the various states in the model, we will also be able to study crossover from “BE-like” to “BCS-like” behaviour. From the point of view of our model, this crossover occurs when going from a situation (*i.e.*, a  $(k, y)$  value) in which  $T_{BE} < T_{SG}$ , to a situation in which masses and binding energies are such that  $T_{SG}$  is smaller than a would-be  $T_{BE}$ . In the latter case, the quantum liquid condensation would

occur simultaneously with the pair formation.

The answer to these questions, and to many others, will require much more future work. However, let us conclude this paper by trying to anticipate our answers to the questions listed in Ref. [5] and quoted in Sect. 1:

- **What is the physical origin of the anomalous *normal* state?** A dynamical, antiferromagnetically interacting spin background, *strongly* coupled to fermions (the *heavy* fermions of the type  $(\boldsymbol{\tau} \cdot \boldsymbol{\phi})\psi$  in our model).
- **What characterizes this anomalous *normal* state?** The presence of heavy, single fermionic charges  $((\boldsymbol{\tau} \cdot \boldsymbol{\phi})\psi)$  and *light, bosonic* charge-2 bound states.
- **What is the mechanism of high- $T_c$  superconductivity?** Bose-Einstein condensation of these dynamically formed, *stable* bosonic charge-2 pairs.
- **What is the pairing state?** A bound state of *heavy* fermions, bound by spin-waves in a *disordered* phase: a **PMS-pair**.

## Acknowledgments

We are indebted to A. Muramatsu and L.A. Fernández for very helpful remarks and stimulating discussions. We also acknowledge interesting discussions with A. Cruz, Ph. de Forcrand, J.M. De Teresa, J.G. Esteve, D. Frenkel, J. Garcia, M.R. Ibarra, R. Mahendiran, R. Navarro, C. Rillo, A. Tarancón and especially G. Sierra. We thank, the RTNN collaboration for computing facilities. This work is financially supported by CICYT (Spain), projects AEN 96-1670, AEN 96-1674, AEN 97-1680 and by Acción Integrada Hispano-Francesa HF1996-0022.

## References

- [1] J.G. Bednorz and K.A. Müller, *Z.Phys.* **B64** (1986) 189.
- [2] M. Randeria, preprint cond-mat/9710223.
- [3] D. Mihailovic *et al*, cond-mat/9801049; H. Ding *et al*, cond-mat/9712100.
- [4] C.C. Tsuei *et al.*, *Science* **271** (1996) 329; M. Sigrist and T.M.Rice, *Rev. Mod. Phys.* **67** (1995) 503; D.J. Van Harlingen, *Rev. Mod. Phys.* **67** (1995) 515.
- [5] D. Pines, preprint cond-mat/9704102.
- [6] F.D.M. Haldane, *Phys. Lett.* **A93** (1983) 464; *Phys. Rev. Lett.* **50** (1983) 1153.
- [7] S. Chakravarty, B.I. Halperin and D.R. Nelson, *Phys. Rev. Lett.* **60** (1988) 1507; *Phys. Rev.* **B39** (1989) 2344.
- [8] P. Hasenfratz and H. Leutwyler, *Nucl. Phys.* **B343** (1990) 241; P. Hasenfratz and F. Niedermayer, *Phys. Lett.* **B268** (1991) 231; P. Hasenfratz and F. Niedermayer, *Z. Phys.* **B92** (1993) 91.
- [9] Y. Endoh *et al.* *Phys. Rev.* **B37** (1988) 7443.
- [10] H.Q. Ding and M.S. Makivic *Phys. Rev. Lett.* **64** (1990) 1449. U.-J. Wiese and H.-P. Ying, *Z. Phys.* **B93** (1994) 147.
- [11] J.L. Alonso, Ph. Boucaud, V. Martín-Mayor and A.J. van der Sijs, preprint cond-mat/9706022, to be published in *Europhys. Lett.*
- [12] J.L. Alonso, Ph. Boucaud, V. Martín-Mayor and A.J. van der Sijs, *Nucl. Phys. B (Proc. Suppl.)* **63** (1998) 658.
- [13] C. Kübert and A. Muramatsu, *Europhys. Lett.* **30** (1995) 481.
- [14] F.C. Zhang and T.M. Rice, *Phys. Rev.* **B37** (1988) 3759.
- [15] G. Parisi, *Nucl. Phys.* **B205** (1982) 337; E. Abdalla, *Phys. Rev.* **D41** (1990) 571.
- [16] A similar result has been found by A.V. Chubukov and D.K. Morr, preprint cond-mat/9701196.
- [17] D.S. Marshall *et al.*, *Phys. Rev. Lett.* **76** (1996) 4841; *Science* **273** (1996) 325.
- [18] N.R. Norman *et al.*, preprint cond-mat/9710163; H. Ding *et al.*, *Phys. Rev. Lett.* **78** (1997) 2628.
- [19] B.B. Beard, R.J. Birgeneau, M. Greven and U.-J. Wiese, preprint cond-mat/9709110.
- [20] J.R. Schrieffer, X.G. Wen and S.C. Zhang, *Phys. Rev. Lett.* **60** (1988) 944; *Phys. Rev.* **B39** (1989) 11663.
- [21] P.W. Anderson and J.R. Schrieffer, *Physics Today*, June 1991, 54.

- [22] R.J. Birgeneau, *Am. J. Phys.* **58** (1) *January 1990*, 28.
- [23] A. Aharony *et al.*, *Phys. Rev. Lett.* **60** (1988) 1330.
- [24] I. Affleck and J.B. Marston, *Phys. Rev.* **B37** (1988) 3774.
- [25] K. Wilson, in *New Phenomena in Sub-Nuclear Physics* (Erice, 1975). L.H. Karsten and J. Smit, *Nucl. Phys.* **B183** (1981) 103; H.B. Nielsen and Ninomiya, *Nucl. Phys.* **B185** (1981) 20 and **B193** (1981) 173, Erratum, *Nucl. Phys.* **B195** (1982) 541.
- [26] A.K. De and J. Jersák, in *Heavy flavours*, ed. A. Buras and M. Lindner (World Scientific Singapore, 1992).
- [27] T.W. Appelquist, M. Bowick, D. Karabali and L.C.R. Wijewardhana, *Phys. Rev.* **D33** (1986) 3704.
- [28] For a review see F. Karsch in *Quark Gluon Plasma*, (World Scientific Singapore, 1990), edited by R.C. Hwa.
- [29] See, *eg*, J. Shigemitsu, *Nucl. Phys. B (Proc. Suppl.)* **20** 515 (1991); W. Bock, *et al.*, *Nucl. Phys.* **B344**, 207 (1990).
- [30] We are indebted to A. Muramatsu for emphasizing this point.
- [31] J.-M. Drouffe and J.-B. Zuber, *Phys. Rep.* **102** (1983) 1.
- [32] J.L. Alonso, Ph. Boucaud, F. Lesmes and E. Rivas, *Phys. Lett.* **B329** (1994) 75.
- [33] J.L. Alonso, Ph. Boucaud, F. Lesmes and A.J. van der Sijs, *Nucl. Phys.* **B457** (1995) 175; **472** (1996) 738 (E).
- [34] R.T. Scalettar, D.J. Scalapino and R.L. Sugar, *Phys. Rev.* **B34** (1986) 7911; S. Duane, A.D. Kennedy, B.J. Pendleton and D. Roweth, *Phys. Lett.* **B195** (1987) 216.
- [35] G. Batrouni *et al.*, *Phys. Rev.* **D32** (1986) 2736; S. Gottlieb, W. Liu, D. Toussaint and R.L. Sugar, *Phys. Rev.* **D35** (1987) 2531.
- [36] I. Montvay and G. Münster, *Quantum Fields on a Lattice* (Cambridge University Press, 1994); H.J. Rothe, *Lattice Gauge Theories – An Introduction* (World Scientific, 1992).
- [37] H. Goldstein, *Classical Mechanics* (Addison-Wesley, 1959).
- [38] H. G. Ballesteros, L. A. Fernández, V. Martín-Mayor and A. Muñoz Sudupe, *Phys. Lett.* **B387** (1996) 125.
- [39] U. Wolff, *Phys. Rev. Lett.* **62** (1989) 3834.
- [40] J. L. Alonso *et al.*, *Phys. Rev.* **B53** (1996) 2537; H. G. Ballesteros, L. A. Fernández, V. Martín-Mayor and A. Muñoz Sudupe, *Phys. Lett.* **B378** (1996) 207.
- [41] R. Gupta *et al.*, *Phys. Rev.* **D40** (1989) 2072.

- [42] M. Falcioni, E. Marinari, M. L. Paciello, G. Parisi and B. Taglienti, *Phys. Lett.* **108** (1982) 331; A. M. Ferrenberg and R. H. Swendsen, *Phys. Rev. Lett.* **61** (1988) 2635.
- [43] M.A. Stephanov and M.M. Tsypin, *Phys. Lett.* **B236** (1990) 344; M.A. Stephanov, *Phys. Lett.* **B266** (1991) 447.
- [44] J. Smit, *Nucl. Phys.* **B (Proc. Suppl.) 9** (1989) 579; M.F.L. Golterman, D.N. Petcher and J. Smit, *Nucl. Phys.* **B370** (1992) 51.
- [45] B. I. Shraiman and E. D. Siggia, *Phys. Rev. Lett.* **62** (1989) 1564.
- [46] Y.Moritomo *et al.*, *Phys. Rev.* **B51** (1995) 3297
- [47] G. Blumberg, M.V. Kleain and S. W. Cheong, *Phys. Rev. Lett.* **80** (1998) 564; J. M. Tranquada, cond-mat/9802043.
- [48] J.H. Brewer *et al.*, *Phys. Rev. Lett.* **60** (1988) 1073.